

Robust Output Tracking for an Uncertain and Nonlinear 3D PDE-ODE System: Preventing Induced Seismicity in Underground Reservoirs

Diego Gutiérrez-Oribio and Ioannis Stefanou

Abstract—This paper presents a robust control strategy for output tracking of a nonlinear 3D PDE-ODE system. The output feedback control was developed by bounding the solution and its time derivative for both the infinite-dimensional system and the nonlinear ODE, and leveraging these bounds to ensure the boundedness of the control coefficient and error dynamics perturbations. The mathematical framework demonstrates the controller's ability to manage two output types within the system, overcoming model uncertainties and heterogeneities using minimal system information and a continuous control signal. A case study addressing induced seismicity mitigation while ensuring energy production in the Groningen gas reservoir highlights the control's effectiveness. The strategy guarantees precise tracking of target seismicity rates and pressures across reservoir regions, even under parameter uncertainties. Numerical simulations validate the approach in two scenarios: gas extraction with minimal seismicity and the addition of CO₂ injections achieving net-zero environmental impact.

Index Terms—Distributed parameter systems, Robust control, Output feedback, Nonlinear systems.

I. INTRODUCTION

IN the realm of dynamic systems, the interplay between time-dependent and spatially-dependent behaviours presents both opportunities and challenges for modelling and control. Ordinary Differential Equations (ODEs) effectively capture the dynamics of systems governed by a single independent variable, typically time, and are widely used in many fields such as physics, engineering, and economics [1]. Conversely, Partial Differential Equations (PDEs) allow for the description of systems where multiple independent variables, including spatial dimensions, significantly influence the behaviour of the system [2]. As a result, ODE-PDE systems have emerged as a powerful framework for modelling complex phenomena that exhibit both temporal evolution and spatial interaction.

These cascade systems are prevalent in various applications, ranging from continuum mechanics, heat transfer and electromagnetism [3], [4], [5]. Their intricate structure necessi-

tates sophisticated control strategies capable of addressing the dynamic coupling between the ODE and PDE components. Some examples of used control techniques are state and output feedback control, backstepping, observer design, and sliding-modes [6], [7], [8], [9], [4], [10].

A PDE-ODE cascade system can also be used to model the probability of seismic events caused by fluid injection or extraction in an underground reservoir. Deep geothermal energy, carbon capture and storage, and hydrogen storage have shown significant potential in meeting the growing demands of the energy sector while reducing CO₂ emissions. However, the effectiveness of these methods hinges on the injection and extraction of fluids into the Earth's crust, a process that may inadvertently induce earthquakes [11], [12], [13]. This concern has resulted in the closure of several geothermal plants worldwide, including those in Alsace, France, in 2020 [14], [15], Pohang, South Korea, in 2019 [16], [17], Basel, Switzerland, in 2009 [18], [19], and the gas reservoir in Groningen, Netherlands, in 2024 [20], [21]. Therefore, effective strategies for earthquake prevention are crucial to mitigate induced seismicity in underground reservoirs. Commonly employed methods, such as traffic light systems, cyclic stimulation, and fracture caging, are among the most prevalent approaches for managing seismic risks [22], [23], [24], [25]. However, these techniques often rely on a trial-and-error approach rather than systematic, mathematically grounded control strategies, which limits their ability to ensure the complete avoidance of induced seismic events [22], [26], [27] and the maximization of production.

In recent years, significant advancements have been made in controlling seismic instabilities in specific, well-characterized, mature faults [28], [29], [30], [31], [32], [33]. These studies have employed various control algorithms to slow the release of accumulated energy at a rate far lower than would occur in natural, uncontrolled seismic events. Furthermore, a robust control method was developed to track the seismicity rate (SR) in underground reservoirs in [34]. However, due to mathematical complexities, this approach was based on simplified region-wise SR models, rather than point-wise, and did not directly control the SR output.

A robust control strategy for output tracking in a nonlinear 3D PDE-ODE system is presented in this paper. The mathematical derivations demonstrate the controller's effectiveness in handling the tracking of two types of outputs within the

This paper was submitted December 10, 2024 for review.

Diego Gutiérrez-Oribio is with Nantes Université, Ecole Centrale Nantes, CNRS, GeM, UMR 6183, F-44000, Nantes, France (e-mail: diego.gutierrez-oribio@ec-nantes.fr). Ioannis Stefanou is with IMSIA (UMR 9219), CNRS, EDF, CEA, ENSTA Paris, Institut Polytechnique de Paris, Palaiseau, France (e-mail: ioannis.stefanou@ensta-paris.fr).

system, despite model uncertainties, heterogeneities in the system, and minimal system information, while utilizing a continuous control signal. Moreover, the control design effectively addressed the complex interconnection between the infinite-dimensional system and a nonlinear ODE in three dimensions. The control approach is demonstrated through a case study focused on preventing induced seismicity while maintaining energy production in a real underground reservoir: the Groningen gas reservoir. Groningen was closed in 2024 after 60 years of operation due to excessive induced seismicity that existing, mostly empirical, methods failed to prevent. Unlike those, the proposed control strategy ensures robust tracking of desired (point-wise) SR and pressures across different regions in the geological reservoir, even in the presence of system uncertainties, while ensuring desired production of gas. More specifically, numerical simulations confirm the theoretical approach using a validated model of the Groningen reservoir under two scenarios. In the first scenario, the same level of gas extraction as in reality is maintained, while preventing earthquake activity, in contrast to actual historical events. In the second scenario, CO₂ injection is incorporated to ensure a zero net carbon impact, optimizing renewable energy production and storage.

The structure of this paper is outlined as follows. Section II introduces the underlying 3D PDE-ODE model and defines the control objectives. In Section III, the output feedback control strategy for robust tracking in this nonlinear and uncertain system is presented. Section IV demonstrates the effectiveness of the proposed control strategy through simulations conducted on a validated model of the Groningen gas reservoir, along with a discussion of the limitations of the approach. Finally, Section V provides concluding remarks, summarizing the key findings of the study.

Notation and used inequalities

We denote by $\|\cdot\|$ the euclidean norm of the n -dimensional Euclidean space, \mathbb{R}^n . \mathbb{I}_n is the $n \times n$ identity matrix and $0_{n \times m}$ is the $n \times m$ zero matrix. The spectral norm of a matrix $A \in \mathbb{R}^{n \times n}$ is defined by $\|A\| = \sqrt{\lambda_{\max}(A^T A)}$, where $\lambda_{\max}(\cdot)$ represents the maximum eigenvalue of the matrix. A column vector $\Phi = [\phi_1, \dots, \phi_m]^T$ is denoted as $\Phi = [\phi_i]_{i=1}^m$ and a diagonal matrix $A = \text{diag}(a_1, \dots, a_m)$ is denoted as $A = \text{diag}(a_i)_{i=1}^m$. The symbol \forall means “for all” and the symbol $\forall\forall$ means “for almost all”. The partial time derivative of $u(x, t)$ is denoted by $u_t = \partial u / \partial t$ and the total time derivative by $\dot{u} = du / dt$. The gradient by $\nabla u = [\partial u / \partial x_1, \dots, \partial u / \partial x_n]$, and the Laplacian by $\nabla^2 u = \nabla u \cdot \nabla u^T = \sum_{i=1}^n \partial^2 u / \partial x_i^2$.

We denote by V an open subset in \mathbb{R}^3 of positive measure and $S = \partial V \in C^{0,1}$ its Lipschitz boundary. We also define $T = [0, \infty)$ as the time domain starting at 0. Consider the scalar functions $u(x, t)$ that belong to the Sobolev space, $\mathcal{W} = C^0(T; H^1(V))$, such that

$$\mathcal{W} = \left\{ u \mid u(x, \cdot), \nabla u(x, \cdot) \in \mathcal{L}^2(V), \right. \\ \left. \|u\|_{H^1(V)} < \infty, \|u_t\|_{H^1(V)} < \infty, \quad \forall\forall t \in T \right\},$$

where $\mathcal{L}^2(V)$ is the space of square-integrable functions over V , $\|u(x, \cdot)\|_{H^1(V)} = \sqrt{\|u(x, \cdot)\|_{H^0(V)}^2 + \|\nabla u(x, \cdot)\|_{H^0(V)}^2}$,

$$\|u(x, \cdot)\|_{H^0(V)} = \sqrt{\int_V [u(x, \cdot)]^2 dV}.$$

Some important inequalities are recalled for their later use: *Poincaré-Wirtinger Inequality*: For $u(x, t) \in \mathcal{W}$ with Lipschitz boundary S , the next inequality is fulfilled:

$$\|u(x, t) - \bar{u}(t)\|_{H^0(V)} \leq \epsilon \|\nabla u(x, t)\|_{H^0(V)}, \quad (1)$$

where

$$\bar{u}(t) = \frac{1}{V} \int_V u(x, t) dV, \quad (2)$$

is the average of $u(x, t)$ over V and $\epsilon > 0$ depends only on V .

Cauchy-Schwarz Inequality:

$$\int_V f(x, t)g(x, t) dV \leq \|f(x, t)\|_{H^0(V)} \|g(x, t)\|_{H^0(V)}, \quad (3)$$

for any $f(x, \cdot), g(x, \cdot) \in \mathcal{L}^2(V)$.

II. PROBLEM STATEMENT

Let the 3D diffusion system be written as follows

$$u_t(x, t) = -\frac{1}{\beta} \nabla q(x, t) + \frac{1}{\beta} \sum_{i=1}^n \mathcal{B}_i(x) Q_i(t), \\ q(x, t) = -\frac{k(x, t)}{\eta(x, t)} \nabla u(x, t), \quad (4) \\ q(x, t) \cdot \hat{e} = 0 \quad \forall x \in S, \\ u(x, 0) = u^0(x) \in \mathcal{L}^2(V),$$

where $u(x, t)$ is the solution evolving within the space \mathcal{W} and $u^0(x)$ its initial condition. $q(x, t)$ is a flux term according to Darcy’s law. Neumann boundary conditions are considered where \hat{e} is a unitary vector normal to S . $\beta > 0$ is a system parameter, and $k(x, t) \in \mathbb{R}^{3 \times 3}$ and $\eta(x, t)$ are system functions that depend on the space and time variables. $Q(t) \in \mathbb{R}^n$, $Q(t) = [Q_1(t), \dots, Q_n(t)]^T$, are flux sources (inputs) applied through the coefficients $\mathcal{B}_i(x)$ defined as

$$\mathcal{B}_i(x) = \begin{cases} \frac{1}{V_i^*} & \text{if } x \in V_i^* \\ 0 & \text{if } x \notin V_i^* \end{cases}, \quad i = 1, \dots, n, \quad V_i^* \subset V. \quad (5)$$

Note that $\mathcal{B}_i(x) \in \mathcal{L}^2(V)$ ($\|\mathcal{B}_i(x)\|_{H^0(V)} = 1/\sqrt{V_i^*}$) and $\int_V \mathcal{B}_i(x) dV = \int_{V_i^*} \mathcal{B}_i(x) dV = 1$ for all $i = 1, \dots, n$. Furthermore, $\mathcal{B}_i(x)$ tends to be a Dirac’s distribution as $V_i^* \rightarrow 0$.

Let the next 3D ODE system be applied in a cascade connection with the diffusion equation as

$$R_t(x, t) = R(x, t) \left\{ -\gamma_1(x, t) u_t(x, t) \right. \\ \left. - \gamma_2(x, t) [R(x, t) - R^*] \right\}, \quad (6)$$

where $R(x, t)$ is the solution evolving within the space $\mathcal{W}_R = \{R \mid \|R\|_{H^1(V)} < \infty, \|R_t\|_{H^1(V)} < \infty, \quad \forall\forall t \in T\}$. $\gamma_1(x, t)$ and $\gamma_2(x, t)$ are system functions that depend on the space and time variables and $R^* > 0$ is a constant value. $u_t(x, t)$ is the input of this system, which is the time derivative of the solution of system (4).

System (4)–(6) can be used to model seismicity rate in underground reservoirs, *i.e.*, the probability of having a seismic

event due to fluid injection and/or extraction. $u(x, t)$ represents the fluid pressure change, $Q(t)$ represents fluxes of fluid (a positive $Q_i(t)$ means injection and a negative $Q_i(t)$ extraction) and $R(x, t)$ represents the SR (see Section IV for more details on the physical interpretation of this problem). Under this sense, the SR can only take positive values, *i.e.*, $R(x, t) > 0 \forall (x, t) \in (V \times T)$.

The objective of this work is to design the control input $Q(t)$ of system (4) to force averages of pressure and SR over some regions of the domain, V , to follow (track) desired references, *i.e.*, to drive the outputs $y_u \in \mathfrak{R}^{m_u}$, $y_u = [y_{u_1}, \dots, y_{u_{m_u}}]^T$, and $y_R \in \mathfrak{R}^{m_R}$, $y_R = [y_{R_1}, \dots, y_{R_{m_R}}]^T$, with components

$$\begin{aligned} y_{u_i}(t) &= \frac{1}{V_{u_i}} \int_{V_{u_i}} u(x, t) dV, \quad V_{u_i} \subset V, \quad i = 1, \dots, m_u, \\ y_{R_i}(t) &= \frac{1}{V_{R_i}} \int_{V_{R_i}} R(x, t) dV, \quad V_{R_i} \subset V, \quad i = 1, \dots, m_R, \end{aligned} \quad (7)$$

to desired references $r_u(t) \in \mathfrak{R}^{m_u}$, $r_u(t) = [r_{u_1}(t), \dots, r_{u_{m_u}}(t)]^T$, and $r_R(t) \in \mathfrak{R}^{m_R}$, $r_R(t) = [r_{R_1}(t), \dots, r_{R_{m_R}}(t)]^T$, respectively.

The control design will be performed under the following assumptions for system (4)–(6):

Assumption 1: The control input is bounded as $\|Q(t)\| \leq L_Q$ for all $t \in T$. Consequently, $\dot{Q}(t)$ and $\ddot{Q}(t)$ cannot be infinite over a finite interval, so it exists $L_{\dot{Q}}, L_{\ddot{Q}} > 0$ such that $\|\dot{Q}(t)\| \leq L_{\dot{Q}}$ and $\|\ddot{Q}(t)\| \leq L_{\ddot{Q}}$ to be fulfilled $\forall t \in T$.

Assumption 2: The references to be followed, $r_u(t)$ and $r_R(t)$, are designed to fulfil

$$\begin{aligned} \|r_u(t)\| &\leq L_{r_u}, \quad \|\dot{r}_u(t)\| \leq L_{\dot{r}_u}, \quad \|\ddot{r}_u(t)\| \leq L_{\ddot{r}_u}, \\ \|r_R(t)\| &\leq L_{r_R}, \quad \|\dot{r}_R(t)\| \leq L_{\dot{r}_R}, \quad \|\ddot{r}_R(t)\| \leq L_{\ddot{r}_R}, \end{aligned} \quad (8)$$

for all $t \in T$.

Assumption 3: The system functions $k(x, t)$, $\eta(x, t)$, $\gamma_1(x, t)$ and $\gamma_2(x, t)$ are uncertain but they fulfil

$$\begin{aligned} 0 < k^m &\leq \|k(x, t)\| \leq k^M, \quad 0 < \gamma_1^m \leq \gamma_1(x, t) \leq \gamma_1^M, \\ 0 < \eta^m &\leq \eta(x, t) \leq \eta^M, \quad 0 < \gamma_2^m \leq \gamma_2(x, t) \leq \gamma_2^M, \\ |\dot{\gamma}_1(x, t)| &\leq L_{\dot{\gamma}_1}, \quad |\dot{\gamma}_2(x, t)| \leq L_{\dot{\gamma}_2}, \end{aligned} \quad (9)$$

for all $(x, t) \in (V \times T)$. Such bounds and the parameter R^* are considered to be known.

Assumption 4: We assume that $V_{u_i} \cap V_{R_j} = \emptyset$, $\forall i = 1, \dots, m_u$ and $\forall j = 1, \dots, m_R$. We also assume that $m = m_u + m_R$ and that there are less outputs than control inputs, *i.e.*, $m \leq n$. Furthermore, there is at least one control input, $Q_i(t)$, $i = 1, \dots, n$, inside every region of the outputs (7), *i.e.*, there exist $i = 1, \dots, m_u$ and $j = 1, \dots, m_R$ such that $V_i^* \subset V_{u_i}$ and $V_j^* \subset V_{R_j}$, for all $V_i^* \cap V_j^* = \emptyset$.

Remark 1: Assumption 1 and 2 are easily met in real control applications where the actuators are saturated and the references to be followed are free to be chosen. Furthermore, assumption 3 involves the physical properties of the real system, which are bounded and, therefore, is always fulfilled.

III. OUTPUT FEEDBACK TRACKING CONTROL DESIGN

Let us define the error variables, $\sigma_u \in \mathfrak{R}^{m_u}$ and $\sigma_R \in \mathfrak{R}^{m_R}$, as follows

$$\begin{aligned} \sigma_u(t) &= y_u(t) - r_u(t), \\ \sigma_R(t) &= \frac{1}{\gamma_{1_0} R^*} [y_R(t) - r_R(t)], \end{aligned} \quad (10)$$

where $\gamma_{1_0} > 0$ is a nominal value of $\gamma_1(x, t)$ that has to be selected. Note that the coefficient $1/\gamma_{1_0} R^*$ was added in the second equation for units consistency.

Using the 3D diffusion equation (4) and the SR system (6), the error dynamics become

$$\begin{aligned} \dot{\sigma}_{u_i}(t) &= -\frac{1}{\beta V_{u_i}} \int_{V_{u_i}} \nabla q(x, t) dV \\ &\quad + \frac{1}{\beta V_{u_i}} \int_{V_{u_i}} \sum_{j=1}^n \mathcal{B}_j(x) Q_j(t) dV - \dot{r}_{u_i}(t), \\ &\quad i = 1, \dots, m_u, \\ \dot{\sigma}_{R_i}(t) &= \frac{1}{\gamma_{1_0} R^* \beta V_{R_i}} \int_{V_{R_i}} \gamma_1(x, t) R(x, t) \nabla q(x, t) dV \\ &\quad - \frac{1}{\gamma_{1_0} R^* \beta V_{R_i}} \int_{V_{R_i}} \gamma_1(x, t) R(x, t) \sum_{j=1}^n \mathcal{B}_j(x) Q_j(t) dV \\ &\quad - \frac{1}{\gamma_{1_0} R^* V_{R_i}} \int_{V_{R_i}} \gamma_2(x, t) R(x, t) [R(x, t) - R^*] dV \\ &\quad - \frac{1}{\gamma_{1_0} R^*} \dot{r}_{R_i}(t), \quad i = 1, \dots, m_R. \end{aligned}$$

In matrix form we have

$$\dot{\sigma}(t) = \Psi(t) + B(t)Q(t), \quad (11)$$

where $\sigma(t) = [\sigma_u(t)^T, \sigma_R(t)^T]^T$, $\Psi(t) \in \mathfrak{R}^m$ is defined as

$$\begin{aligned} \Psi(t) &= \begin{bmatrix} \psi_1(t) \in \mathfrak{R}^{m_u} \\ \psi_2(t) \in \mathfrak{R}^{m_R} \end{bmatrix}, \\ \psi_1(t) &= \left[-\frac{1}{\beta V_{u_i}} \int_{V_{u_i}} \nabla q(x, t) dV - \dot{r}_{u_i}(t) \right]_{i=1}^{m_u}, \\ \psi_2(t) &= \left[\begin{array}{l} \frac{1}{\gamma_{1_0} R^* \beta V_{R_i}} \int_{V_{R_i}} \gamma_1(x, t) R(x, t) \nabla q(x, t) dV \\ - \frac{1}{\gamma_{1_0} R^* V_{R_i}} \int_{V_{R_i}} \gamma_2(x, t) [R(x, t)]^2 dV \\ + \frac{1}{\gamma_{1_0} V_{R_i}} \int_{V_{R_i}} \gamma_2(x, t) R(x, t) dV - \frac{1}{\gamma_{1_0} R^*} \dot{r}_{R_i}(t) \end{array} \right]_{i=1}^{m_R}, \end{aligned} \quad (12)$$

and $B(t) \in \mathfrak{R}^{m \times n}$ is defined as $B(t) = [B_u, B_R(t)]^T$ with $B_u = [b_{ij}^u] \in \mathfrak{R}^{m_u \times n}$, $B_R(t) = [b_{ij}^R(t)] \in \mathfrak{R}^{m_R \times n}$ defined as

$$\begin{aligned} b_{ij}^u &= \begin{cases} \frac{1}{\beta V_{u_i}} & \text{if } V_j^* \subset V_{u_i}, \quad i = 1, \dots, m_u, \\ 0 & \text{if } V_j^* \not\subset V_{u_i}, \quad j = 1, \dots, n, \end{cases} \\ b_{ij}^R(t) &= \begin{cases} -\frac{1}{\gamma_{1_0} R^* \beta V_{R_i} V_j^*} \int_{V_j^*} \gamma_1(x, t) R(x, t) dV & \text{if } V_j^* \subset V_{R_i} \\ 0 & \text{if } V_j^* \not\subset V_{R_i}, \end{cases} \\ &\quad i = 1, \dots, m_R \\ &\quad j = 1, \dots, n. \end{aligned} \quad (13)$$

where the definition of $\mathcal{B}_i(x)$ in (5) has been used.

The matrix $B(t)$ is required to be composed as

$$B(t) = [\mathbb{I}_m + \Delta B(t)] B_0, \quad (14)$$

where $\Delta B(t) \in \mathfrak{R}^{m \times m}$ is the uncertain control coefficient and $B_0 \in \mathfrak{R}^{m \times n}$ is the nominal (known) control coefficient. The matrix B_0 is chosen as $B_0 = [B_{u_0}, B_{R_0}]^T$ with $B_{u_0} = [b_{ij}^{u_0}] \in \mathfrak{R}^{m_u \times n}$, $B_{R_0} = [b_{ij}^{R_0}] \in \mathfrak{R}^{m_R \times n}$ defined as

$$b_{ij}^{u_0} = \begin{cases} \frac{1}{\beta_0 V_{u_i}} & \text{if } V_j^* \subset V_{u_i} \\ 0 & \text{if } V_j^* \not\subset V_{u_i} \end{cases}, \quad i = 1, \dots, m_u, \quad j = 1, \dots, n, \quad (15)$$

$$b_{ij}^{R_0} = \begin{cases} -\frac{1}{\beta_0 V_{R_i}} & \text{if } V_j^* \subset V_{R_i} \\ 0 & \text{if } V_j^* \not\subset V_{R_i} \end{cases}, \quad i = 1, \dots, m_R, \quad j = 1, \dots, n.$$

where $\beta_0 > 0$ is a nominal value of β that has to be selected. Notice that all the nominal matrices are constant and, as such, they require minimum measurements on (11), *i.e.*, we do not need to measure the terms $\int_{V_j^*} \gamma_1(x, t) R(x, t) dV$, $j = 1, \dots, n$ in (13).

Let us choose the control $Q(t)$ as

$$Q(t) = B_0^+ [-k_1 \phi_1(\sigma(t)) + b\nu(t)], \quad (16)$$

$$\dot{\nu}(t) = -k_2 \phi_2(\sigma(t)),$$

where

$$\phi_1(\sigma(t)) = \left(\alpha_1 \|\sigma(t)\|^{-\frac{1}{2}} + \alpha_2 \right) \sigma(t), \quad (17)$$

$$\phi_2(\sigma(t)) = \left(\frac{1}{2} \alpha_1 \|\sigma(t)\|^{-\frac{1}{2}} + \alpha_2 \right) \phi_1(\sigma(t)),$$

and $k_1, k_2, b, \alpha_1, \alpha_2$ are positive constants to be designed. Such control is known as a Multi-Input-Multi-Output (MIMO) Generalized Super-Twisting [35], [36]. The matrix $B_0^+ \in \mathfrak{R}^{m \times m}$ is the right pseudoinverse of B_0 , which always exists due to Assumption 4. The control signal generated is always continuous despite having a discontinuous integral term. In this case, the solutions of (11) are understood in the sense of Filippov [37] (see [38] for details on Filippov solutions for PDE systems like (4)). Such control can be generalized as a homogeneous algorithm (*e.g.*, [35], [34]) to include more cases than the discontinuous case but it exceeds the scope of the current work. Note how the controller is designed with minimum information about the system (11), *i.e.*, with only the measurement of $\sigma(t)$ and the knowledge of the nominal matrix B_0 .

Remark 2: The control input (16) fulfils Assumption 1 if $\|[\sigma^T, \nu^T]^T\| \leq L$, for some $L > 0$, *i.e.*, only local results are on play.

The tracking result for system (11) is then in force.

Theorem 1: Let system (11) under Assumptions 1–4 be driven by the control (16), (17) with $\alpha_1 > 0$, $\alpha_2 > 0$ and $b > 0$. Suppose that the uncertain control coefficient $\Delta B(t)$ in (14) and the perturbation term $\Psi(t)$ in (11) are assumed to fulfil

$$\|\Delta B(t)\| \leq \delta_B < 1, \quad (18)$$

$$\Psi(t) = \Psi_1(t) + \Psi_2(t), \quad (19)$$

$$\|\Psi_1(t)\| \leq \delta_1 \|\sigma(t)\|^{\frac{1}{2}} + \delta_2 \|\sigma(t)\|, \quad (20)$$

$$\left\| \frac{d}{dt} \left[\frac{1}{b} (\mathbb{I}_m + \Delta B(t))^{-1} \Psi_2(t) \right] \right\| \leq \delta_3 + \delta_4 \|\sigma(t)\|, \quad (21)$$

$\forall \forall t \in T$ and positive constants $\delta_B < 1, \delta_1, \delta_2, \delta_3, \delta_4$. Then, there exist positive gains k_1, k_2 defined as

$$k_1 = l\bar{k}_1, \quad k_2 = l^2\bar{k}_2, \quad \bar{k}_1 > \sqrt{\frac{b\bar{k}_2}{1 - \delta_B}}, \quad \bar{k}_2 > 0, \quad (22)$$

where $l > 0$ is sufficiently large, such that the origin of system (11) is locally stable in finite-time.

Proof: Defining a new variable $\sigma_I(t) = \nu(t) + \bar{\Psi}_2(t)$, $\bar{\Psi}_2(t) = \frac{1}{b} [\mathbb{I}_m + \Delta B(t)]^{-1} \Psi_2(t)$, the closed-loop system (11)–(16) can be written as

$$\dot{\sigma} = \Psi_1(t) + [\mathbb{I}_m + \Delta B(t)] [-k_1 \phi_1(\sigma) + b\sigma_I], \quad (23)$$

$$\dot{\sigma}_I = -k_2 \phi_2(\sigma) + \dot{\bar{\Psi}}_2(t).$$

Note that the matrix $\mathbb{I}_m + \Delta B(t)$ has always inverse due to the existence of the pseudoinverse of B_0 and equation (14).

Following [36], the trajectories $[\sigma^T, \sigma_I^T]^T$ of system (23) are ensured to reach the origin for $k_1 > 0$ and $k_2 > 0$ designed as (22) if the conditions (18)–(21) are fulfilled. The proof existence of such bounds is divided in the following four parts for ease of reference. First, we will analyse the diffusion equation (4) to obtain an ISS bound of the pressure and pressure rate w.r.t. to the input $Q(t)$. Second, the SR system (6) will be studied to bound the SR solution w.r.t. to the bounds obtained in the first part. Finally, these bounds will be used to prove the conditions (18)–(21) of the uncertain control coefficient and the perturbation term. **Boundedness of $\|u(x, t)\|_{H^0(V)}$, $\|u_t(x, t)\|_{H^0(V)}$ and $\|u_{tt}(x, t)\|_{H^0(V)}$**

Introducing the next change of coordinates

$$p(x, t) = u(x, t) - \bar{u}(t) = u(x, t) - \frac{1}{V} \int_V u(x, t) dV, \quad (24)$$

system (4) is transformed into

$$p_t(x, t) = -\frac{1}{\beta} \nabla q(x, t) + \frac{1}{\beta} \sum_{i=1}^n \left[\mathcal{B}_i(x) - \frac{1}{V} \right] Q_i(t),$$

$$q(x, t) = -\frac{k(x, t)}{\eta(x, t)} \nabla p(x, t), \quad (25)$$

$$q(x, t) \cdot \hat{e} = 0 \quad \forall \quad x \in S,$$

$$p(x, 0) = u^0(x) - \bar{u}(0) \in \mathcal{L}^2(V).$$

Note that the average of $p(x, t)$ over V is equal to zero, *i.e.*, $\bar{p}(t) = \frac{1}{V} \int_V p(x, t) dV = 0$, which will be use later.

Consider the positive definite and radially unbounded Lyapunov functional candidate

$$\mathcal{V} = \frac{1}{2} \|p(x, t)\|_{H^0(V)}^2. \quad (26)$$

Its time derivative along the trajectories of system (25) reads

$$\dot{\mathcal{V}} = \int_V p(x, t) p_t(x, t) dV$$

$$= -\frac{1}{\beta} \int_V p(x, t) \nabla q(x, t) dV$$

$$+ \frac{1}{\beta} \int_V p(x, t) \sum_{i=1}^n \left[\mathcal{B}_i(x) - \frac{1}{V} \right] Q_i(t) dV.$$

Applying integration by parts, the divergence theorem and the BC on the first term, and the Cauchy-Schwarz inequality (3) on the second term, it follows that

$$\begin{aligned} \dot{\mathcal{V}} &\leq -\frac{1}{\beta} \int_V \nabla \cdot [p(x,t)q(x,t)] dV \\ &\quad - \frac{1}{\beta} \int_V \frac{k(x,t)}{\eta(x,t)} [\nabla p(x,t)]^2 dV \\ &\quad + \frac{1}{\beta} \sum_{i=1}^n \left(\frac{1}{\sqrt{V_i^*}} - \frac{1}{\sqrt{V}} \right) |Q_i(t)| \|p(x,t)\|_{H^0(V)} \\ &\leq -\frac{1}{\beta} \int_S p(x,t) [q(x,t) \cdot \hat{e}] dS - \frac{k^m}{\beta\eta^M} \|\nabla p(x,t)\|_{H^0(V)}^2 \\ &\quad + \frac{\sqrt{n}}{\beta\sqrt{V_T^*}} \|p(x,t)\|_{H^0(V)} \|Q(t)\| \\ &\leq -\frac{k^m}{\beta\eta^M} \|\nabla p(x,t)\|_{H^0(V)}^2 + \frac{\sqrt{n}}{\beta\sqrt{V_T^*}} \|p(x,t)\|_{H^0(V)} \|Q(t)\|, \end{aligned}$$

where $\frac{1}{\sqrt{V_T^*}} = \sum_{i=1}^n \left(\frac{1}{\sqrt{V_i^*}} - \frac{1}{\sqrt{V}} \right)$ and Assumption 3 has been used. Using Poincaré'-Wirtinger inequality (1) (remembering that $\bar{p}(t) = 0$) and the definition of the Lyapunov functional (26), the derivative can be upper-estimated as

$$\begin{aligned} \dot{\mathcal{V}} &\leq -\frac{k^m}{\epsilon\beta\eta^M} \|p(x,t)\|_{H^0(V)}^2 + \frac{\sqrt{n}}{\beta\sqrt{V_T^*}} \|p(x,t)\|_{H^0(V)} \|Q(t)\| \\ &\leq -\frac{2k^m}{\epsilon\beta\eta^M} \mathcal{V} + \frac{\sqrt{2n}}{\beta\sqrt{V_T^*}} L_Q \sqrt{\mathcal{V}}, \end{aligned}$$

where Assumption 1 has been used.

It can be upper bounded as follows (see the comparison lemma in [1])

$$\sqrt{\mathcal{V}(t)} \leq e^{-\frac{k^m}{\epsilon\beta\eta^M} t} \sqrt{\mathcal{V}(0)} + \frac{\epsilon\eta^M \sqrt{n}}{k^m \sqrt{2V_T^*}} L_Q \left(1 - e^{-\frac{k^m}{\epsilon\beta\eta^M} t} \right).$$

Using again the definition of the Lyapunov functional (26), the following bound can be obtained

$$\begin{aligned} \|p(x,t)\|_{H^0(V)} &\leq e^{-\frac{k^m}{\epsilon\beta\eta^M} t} \|p(x,0)\|_{H^0(V)} \\ &\quad + \frac{\epsilon\eta^M \sqrt{n}}{k^m \sqrt{V_T^*}} L_Q \left(1 - e^{-\frac{k^m}{\epsilon\beta\eta^M} t} \right), \end{aligned}$$

which guarantees the global exponential Input-to-State-Stability (eISS) of (25) w.r.t. L_Q (see [31], [39] for more details on eISS on PDE systems). A uniform bound over the solution of system (25) can be obtained as

$$\|p(x,t)\|_{H^0(V)} \leq \|p(x,0)\|_{H^0(V)} + \frac{\epsilon\eta^M \sqrt{n}}{k^m \sqrt{V_T^*}} L_Q, \quad (27)$$

for all $t \in T$.

A similar procedure can be performed to obtain a bound of the norm of $p_t(x,t)$. Indeed, using $\mathcal{V} = \frac{1}{2} \|p_t(x,t)\|_{H^0(V)}^2$ and derivating w.r.t. the time system (25) and Poincaré'-Wirtinger inequality (1) yields

$$\begin{aligned} \|p_t(x,t)\|_{H^0(V)} &\leq e^{-\frac{k^m}{\epsilon\beta\eta^M} t} \|p_t(x,0)\|_{H^0(V)} \\ &\quad + \frac{\epsilon\eta^M \sqrt{n}}{k^m \sqrt{V_T^*}} L_Q \left(1 - e^{-\frac{k^m}{\epsilon\beta\eta^M} t} \right) \\ &\leq \frac{\epsilon\eta^M \sqrt{n}}{k^m \sqrt{V_T^*}} L_Q, \quad \forall t \in T. \end{aligned} \quad (28)$$

In order to obtain a similar bound over the original system (4), let us calculate $\bar{u}_t(t)$ from (4) and (24)

$$\begin{aligned} \bar{u}_t(t) &= \frac{1}{V} \int_V u_t(x,t) dV \\ &= -\frac{1}{\beta V} \int_V \nabla q(x,t) dV + \frac{1}{\beta V} \int_V \sum_{i=1}^n \mathcal{B}_i(x) Q_i(t) dV \\ &= -\frac{1}{\beta V} \int_S q(x,t) \cdot \hat{e} dS + \frac{1}{\beta V} \sum_{i=1}^n Q_i(t) \\ &= \frac{1}{\beta V} \sum_{i=1}^n Q_i(t), \end{aligned} \quad (29)$$

where the divergence theorem and the BC were used.

Finally, using (24), (28) and (29), a uniform bound over the solution rate of system (4) can be obtained as

$$\begin{aligned} \|u_t(x,t)\|_{H^0(V)} &= \|p_t(x,t) + \bar{u}_t(t)\|_{H^0(V)} \\ &\leq \|p_t(x,t)\|_{H^0(V)} + \|\bar{u}_t(t)\|_{H^0(V)} \\ &\leq \frac{\epsilon\eta^M \sqrt{n}}{k^m \sqrt{V_T^*}} L_Q + \frac{1}{\beta\sqrt{V}} \left| \sum_{i=1}^n Q_i(t) \right| \\ &\leq \frac{\epsilon\eta^M \sqrt{n}}{k^m \sqrt{V_T^*}} L_Q + \frac{\sqrt{n}}{\beta\sqrt{V}} L_Q \\ &\leq \Gamma_{u_t} < \infty, \quad \forall t \in T, \end{aligned} \quad (30)$$

for $\Gamma_{u_t} > 0$ due to Assumption 1.

Likewise, a bound over $\|u_{tt}(x,t)\|_{H^0(V)}$ can be found as

$$\begin{aligned} \|u_{tt}(x,t)\|_{H^0(V)} &\leq \frac{\epsilon\eta^M \sqrt{n}}{k^m \sqrt{V_T^*}} L_Q + \frac{\sqrt{n}}{\beta\sqrt{V}} L_Q \\ &\leq \Gamma_{u_{tt}} < \infty, \quad \forall t \in T. \end{aligned} \quad (31)$$

A direct consequence of the bound (30) is that the set of points where the solution rate is unbounded (*i.e.*, $|u_t(x,t)| \rightarrow \infty$) must have zero measure. Indeed, let us assume that there exists a set $V_b \subseteq V$ with positive measure where $|u_t(x,t)| \rightarrow \infty$ for some $t \in T$. Consequently,

$$\int_{V_b} [u_t(x,t)]^2 dV \rightarrow \infty, \quad \text{as } |u_t(x,t)| \rightarrow \infty.$$

Splitting the domain V into $V_c = V \setminus V_b$ (where $|u_t(x,t)| < \infty$) and V_b , we have

$$\begin{aligned} \|u_t(x,t)\|_{H^0(V)}^2 &= \int_{V_c} [u_t(x,t)]^2 dV + \int_{V_b} [u_t(x,t)]^2 dV \\ &\rightarrow \infty, \end{aligned}$$

contradicting the uniform bound (30).

Furthermore, let $V'_c = V_b$, the subset where $|u_t(x,t)| \geq c$ for some $c > 0$. Then

$$\int_{V_b} [u_t(x,t)]^2 dV \geq \int_{V'_c} c^2 dV = c^2 V'_c,$$

where V'_c is the measure of the set V_b . Combining this with the bound (30) gives $V'_c \leq \Gamma_{u_t}^2 / c^2$. As $c \rightarrow \infty$, the measure V'_c (and hence V_b) approaches zero

$$\lim_{c \rightarrow \infty} V'_c \leq 0, \quad \forall t \in T. \quad (32)$$

Therefore, the set of points where $|u_t(x, t)| \rightarrow \infty$ must have measure zero. \square

Boundedness of $\|R(x, t)\|_{H^0(V)}$ and $\|R_t(x, t)\|_{H^0(V)}$

Using the change of coordinates $R(x, t) = e^{h(x, t)}$, system (6) can be transformed to

$$h_t(x, t) = -\gamma_1(x, t)u_t(x, t) - \gamma_2(x, t) \left[e^{h(x, t)} - R^* \right].$$

Using the fact that $h(x, t) \leq e^{h(x, t)} - 1$ for all $(x, t) \in (V \times T)$, the latter system can be upper bounded as follows

$$h_t(x, t) \leq -\gamma_1(x, t)u_t(x, t) - \gamma_2(x, t) [h(x, t) + 1 - R^*].$$

Introducing the change of coordinates $\hat{h}(x, t) = h(x, t) - R^* + 1$ results in the shifted system

$$\hat{h}_t(x, t) \leq -\gamma_1(x, t)u_t(x, t) - \gamma_2(x, t)\hat{h}(x, t).$$

Using the Lyapunov function $\mathcal{V}_h(t) = 1/2[\hat{h}(x, t)]^2$, the comparison lemma [1], Assumption 3, and remembering that $|u_t(x, t)| < c$ with $c > 0$, almost everywhere, (i.e., $u_t(x, t)$ can be unbounded only over a set of zero measure (32)), the trajectories of the latter system can be bounded as

$$\begin{aligned} |\hat{h}(x, t)| &\leq e^{-\gamma_2^m t} |\hat{h}(x, 0)| + (1 - e^{-\gamma_2^m t}) \frac{\gamma_1^M}{\gamma_2^m} c, \\ &\leq |\hat{h}(x, 0)| + \frac{\gamma_1^M}{\gamma_2^m} c, \quad \forall (x, t) \in (V \times T). \end{aligned}$$

Using again the change of coordinates $\hat{h}(x, t) = h(x, t) - R^* + 1$ and the triangle inequality, a bound over $h(x, t)$ can be found

$$\begin{aligned} |h(x, t)| &\leq |h(x, 0)| + 2(R^* + 1) + \frac{\gamma_1^M}{\gamma_2^m} c, \\ &\quad \forall (x, t) \in (V \times T). \end{aligned}$$

Consequently, the norm of $R(x, t)$ can be bounded as

$$\begin{aligned} \|R(x, t)\|_{H^0(V)} &= \left\| e^{h(x, t)} \right\|_{H^0(V)} \\ &< \left\| e^{|h(x, 0)|} e^{2(R^* + 1) + \frac{\gamma_1^M}{\gamma_2^m} c} \right\|_{H^0(V)} \quad (33) \\ &< e^{2(R^* + 1) + \frac{\gamma_1^M}{\gamma_2^m} c} \left\| e^{|\ln(R(x, 0))|} \right\|_{H^0(V)} \\ &\leq \Gamma_R < \infty, \quad \forall t \in T, \end{aligned}$$

for $\Gamma_R > 0$.

Moreover, (6) yields

$$R_t(x, t) \leq -\gamma_1(x, t)R(x, t)u_t(x, t) + \gamma_2(x, t)R(x, t)R^*,$$

and we can obtain a bound of $\|R_t(x, t)\|_{H^0(V)}$ as follows

$$\begin{aligned} \|R_t(x, t)\|_{H^0(V)} &\leq \|\gamma_1(x, t)R(x, t)u_t(x, t)\|_{H^0(V)} \\ &\quad + \|\gamma_2(x, t)R(x, t)R^*\|_{H^0(V)} \\ &\leq \gamma_1^M \|R(x, t)\|_{H^0(V)} \|u_t(x, t)\|_{H^0(V)} \\ &\quad + \gamma_2^M R^* \|R(x, t)\|_{H^0(V)} \\ &\leq \Gamma_R (\gamma_1^M \Gamma_{u_t} + \gamma_2^M R^*) \\ &\leq \Gamma_{R_t} < \infty, \quad \forall t \in T, \end{aligned} \quad (34)$$

for $\Gamma_{R_t} > 0$, where the bounds (30), (33) and Assumption 3 have been used. \square

Uncertain control coefficient boundedness

We will prove condition (18) for the most restrictive case in terms of control, i.e., where the number of inputs and outputs is the same ($n = m$). A similar procedure can be done when there are more control inputs than outputs ($n > m$). Let us begin by splitting the control in $Q(t) = [Q_{u_1}(t), \dots, Q_{u_{m_u}}(t), Q_{R_1}(t), \dots, Q_{R_{m_R}}(t)]^T$. Then, the matrix $B(t)$ in (13) is written as

$$\begin{aligned} B(t) &= \begin{bmatrix} B_u \in \mathbb{R}^{m_u \times m_u} & 0_{m_u \times m_R} \\ 0_{m_R \times m_u} & B_R(t) \in \mathbb{R}^{m_R \times m_R} \end{bmatrix}, \\ B_u &= \text{diag} \left(\frac{1}{\beta V_{u_i}} \right)_{i=1}^{m_u}, \\ B_R(t) &= \text{diag} \left(-\frac{1}{\gamma_{10} R^* \beta V_{R_i} V_{R_i}^*} \int_{V_{R_i}^*} \gamma_1(x, t) R(x, t) dV \right)_{i=1}^{m_R}. \end{aligned} \quad (35)$$

Likewise, the nominal matrix B_0 in (15) is written as

$$\begin{aligned} B_0 &= \begin{bmatrix} B_{u_0} \in \mathbb{R}^{m_u \times m_u} & 0_{m_u \times m_R} \\ 0_{m_R \times m_u} & B_{R_0} \in \mathbb{R}^{m_R \times m_R} \end{bmatrix}, \\ B_{u_0} &= \text{diag} \left(\frac{1}{\beta_0 V_{u_i}} \right)_{i=1}^{m_u}, \\ B_{R_0} &= \text{diag} \left(-\frac{1}{\beta_0 V_{R_i}} \right)_{i=1}^{m_R}, \end{aligned} \quad (36)$$

and $\Delta B(t)$ can be obtained from (14), (35) and (36) as follows

$$\begin{aligned} \Delta B(t) &= \begin{bmatrix} \Delta B_u \in \mathbb{R}^{m_u \times m_u} & 0_{m_u \times m_R} \\ 0_{m_R \times m_u} & \Delta B_R(t) \in \mathbb{R}^{m_R \times m_R} \end{bmatrix}, \\ \Delta B_u &= B_u B_{u_0}^{-1} - \mathbb{I}_{m_u} = \text{diag} \left(\frac{\beta_0}{\beta} - 1 \right)_{i=1}^{m_u}, \\ \Delta B_R(t) &= B_R(t) B_{R_0}^{-1} - \mathbb{I}_{m_R} \\ &= \text{diag} \left(\frac{\beta_0}{\beta \gamma_{10} R^* V_{R_i}^*} \int_{V_{R_i}^*} \gamma_1(x, t) R(x, t) dV - 1 \right)_{i=1}^{m_R}. \end{aligned} \quad (37)$$

In order to prove (18), let us calculate the spectral norm of (37)

$$\begin{aligned} \|\Delta B(t)\| &= \max_{i=1, \dots, m_R} \left\{ \left| \frac{\beta_0}{\beta} - 1 \right|, \right. \\ &\quad \left. \left| \frac{\beta_0}{\beta \gamma_{10} R^* V_{R_i}^*} \int_{V_{R_i}^*} \gamma_1(x, t) R(x, t) dV - 1 \right| \right\} \\ &\leq \max_{i=1, \dots, m_R} \left\{ \left| \frac{\beta_0}{\beta} - 1 \right|, \right. \\ &\quad \left. \left| \frac{\beta_0 \gamma_1^M}{\beta \gamma_{10} R^* \sqrt{V_{R_i}^*}} \|R(x, t)\|_{H^0(V)} - 1 \right| \right\} \end{aligned}$$

where Cauchy-Schwarz Inequality (3) has been used. Finally, using the bound of $\|R(x, t)\|_{H^0(V)}$ in (33) we can obtain

$$\begin{aligned} \|\Delta B(t)\| &\leq \max_{i=1, \dots, m_R} \left\{ \left| \frac{\beta_0}{\beta} - 1 \right|, \left| \frac{\beta_0 \gamma_1^M}{\beta \gamma_{10} R^* \sqrt{V_{R_i}^*}} \Gamma_R - 1 \right| \right\} \\ &\leq \delta_B, \quad \forall t \in T, \end{aligned}$$

which always fulfils (18) if β_0 and γ_{1_0} are selected such as

$$\beta_0 < 2\beta, \quad \gamma_{1_0} > \frac{\gamma_1^M \Gamma_R}{R^* \min_{i=1, \dots, m_R} \{\sqrt{V_{R_i}^*}\}}. \quad (38)$$

□

Perturbation Boundedness

We start by splitting the term $\Psi(t)$ in (12) as shown in (19) with $\Psi_1(t)$ defined as

$$\begin{aligned} \Psi_1(t) &= \begin{bmatrix} \psi_{11}(t) \in \mathfrak{R}^{m_u} \\ \psi_{21}(t) \in \mathfrak{R}^{m_R} \end{bmatrix}, \\ \psi_{12}(t) &= 0_{m_u \times 1}, \\ \psi_{21}(t) &= \left[\frac{1}{\gamma_{1_0} V_{R_i}} \int_{V_{R_i}} \gamma_2(x, t) R(x, t) dV - \frac{\gamma_2^M}{\gamma_{1_0}} r_{R_i}(t) \right]_{i=1}^{m_R}, \end{aligned}$$

and $\Psi_2(t)$ defined as

$$\begin{aligned} \Psi_2(t) &= \begin{bmatrix} \psi_{12}(t) \in \mathfrak{R}^{m_u} \\ \psi_{22}(t) \in \mathfrak{R}^{m_R} \end{bmatrix}, \\ \psi_{12}(t) &= \left[-\frac{1}{\beta V_{u_i}} \int_{V_{u_i}} \nabla q(x, t) dV - \dot{r}_{u_i}(t) \right]_{i=1}^{m_u}, \\ \psi_{22}(t) &= \left[\begin{array}{l} \frac{1}{\gamma_{1_0} R^* \beta V_{R_i}} \int_{V_{R_i}} \gamma_1(x, t) R(x, t) \nabla q(x, t) dV \\ - \frac{1}{\gamma_{1_0} R^* V_{R_i}} \int_{V_{R_i}} \gamma_2(x, t) [R(x, t)]^2 dV \\ + \frac{\gamma_2^M}{\gamma_{1_0}} r_{R_i}(t) - \frac{1}{\gamma_{1_0} R^*} \dot{r}_{R_i}(t) \end{array} \right]_{i=1}^{m_R}. \end{aligned} \quad (39)$$

Using Assumption 3 and the definitions (7) and (10), the norm of the first term is calculated as follows

$$\begin{aligned} \|\Psi_1(t)\| &= \sqrt{\sum_{i=1}^{m_R} \left(\frac{1}{\gamma_{1_0} V_{R_i}} \int_{V_{R_i}} \gamma_2(x, t) R(x, t) dV - \frac{\gamma_2^M}{\gamma_{1_0}} r_{R_i}(t) \right)^2} \\ &\leq \sqrt{\sum_{i=1}^{m_R} \left(\frac{\gamma_2^M}{\gamma_{1_0} V_{R_i}} \int_{V_{R_i}} R(x, t) dV - \frac{\gamma_2^M}{\gamma_{1_0}} r_{R_i}(t) \right)^2} \\ &\leq \sqrt{\sum_{i=1}^{m_R} \left(\frac{\gamma_2^M}{\gamma_{1_0}} y_{R_i}(t) - \frac{\gamma_2^M}{\gamma_{1_0}} r_{R_i}(t) \right)^2} \\ &\leq \sqrt{\sum_{i=1}^{m_R} (\gamma_2^M R^* \sigma_{R_i}(t))^2} \\ &\leq \gamma_2^M R^* \|\sigma_R(t)\| \leq \gamma_2^M R^* \|\sigma(t)\|, \end{aligned}$$

which clearly satisfies (20) with any $\delta_1 > 0$ and $\delta_2 \geq \gamma_2^M R^*$.

Calculating the norm of the term $\Psi_2(t)$ results in

$$\begin{aligned} \|\Psi_2(t)\| &= \left[\sum_{i=1}^{m_u} \left(-\frac{1}{\beta V_{u_i}} \int_{V_{u_i}} \nabla q(x, t) dV - \dot{r}_{u_i}(t) \right)^2 \right. \\ &\quad + \sum_{i=1}^{m_R} \left(\frac{1}{\gamma_{1_0} R^* \beta V_{R_i}} \int_{V_{R_i}} \gamma_1(x, t) R(x, t) \nabla q(x, t) dV \right. \\ &\quad - \frac{1}{\gamma_{1_0} R^* V_{R_i}} \int_{V_{R_i}} \gamma_2(x, t) [R(x, t)]^2 dV \\ &\quad \left. \left. + \frac{\gamma_2^M}{\gamma_{1_0}} r_{R_i}(t) - \frac{1}{\gamma_{1_0} R^*} \dot{r}_{R_i}(t) \right)^2 \right]^{\frac{1}{2}} \\ &\leq \left[\sum_{i=1}^{m_u} \left(\frac{1}{\beta^2 V_{u_i}} \int_{V_{u_i}} [\nabla q(x, t)]^2 dV + \dot{r}_{u_i}^2(t) \right) \right. \\ &\quad + \sum_{i=1}^{m_R} \left(\frac{\gamma_1^M}{\gamma_{1_0}^2 R^* \beta^2 V_{R_i}^2} \int_{V_{R_i}} [R(x, t)]^2 [\nabla q(x, t)]^2 dV \right. \\ &\quad + \frac{\gamma_2^M}{\gamma_{1_0}^2 R^* V_{R_i}^2} \left(\int_{V_{R_i}} [R(x, t)]^2 dV \right)^2 \\ &\quad \left. \left. + \frac{\gamma_2^M}{\gamma_{1_0}^2} r_{R_i}^2(t) + \frac{1}{\gamma_{1_0}^2 R^*} \dot{r}_{R_i}^2(t) \right) \right]^{\frac{1}{2}}. \end{aligned}$$

Defining $\frac{1}{V_{u_T}} = \sum_{i=1}^{m_u} \frac{1}{V_{u_i}}$ and $\frac{1}{V_{R_T}^2} = \sum_{i=1}^{m_R} \frac{1}{V_{R_i}^2}$, the latter expression can be reduced to

$$\begin{aligned} \|\Psi_2(t)\| &\leq \left[\frac{m_u}{\beta^2 V_{u_T}} \|\nabla q(x, t)\|_{H^0(V)}^2 + \|\dot{r}_u(t)\|^2 \right. \\ &\quad + \frac{\gamma_1^M m_R}{\gamma_{1_0}^2 R^* \beta^2 V_{R_T}^2} \|R(x, t)\|_{H^0(V)}^2 \|\nabla q(x, t)\|_{H^0(V)}^2 \\ &\quad + \frac{\gamma_2^M m_R}{\gamma_{1_0}^2 R^* V_{R_T}^2} \|R(x, t)\|_{H^0(V)}^4 \\ &\quad \left. + \frac{\gamma_2^M}{\gamma_{1_0}^2} \|r_R(t)\|^2 + \frac{1}{\gamma_{1_0}^2 R^*} \|\dot{r}_R(t)\|^2 \right]^{\frac{1}{2}} \\ &\leq \frac{\sqrt{m_u}}{\beta \sqrt{V_{u_T}}} \|\nabla q(x, t)\|_{H^0(V)} + \|\dot{r}_u(t)\| \\ &\quad + \frac{\gamma_1^M \sqrt{m_R}}{\gamma_{1_0} R^* \beta V_{R_T}} \|R(x, t)\|_{H^0(V)} \|\nabla q(x, t)\|_{H^0(V)} \\ &\quad + \frac{\gamma_2^M \sqrt{m_R}}{\gamma_{1_0} R^* V_{R_T}} \|R(x, t)\|_{H^0(V)}^2 \\ &\quad + \frac{\gamma_2^M}{\gamma_{1_0}} \|r_R(t)\| + \frac{1}{\gamma_{1_0} R^*} \|\dot{r}_R(t)\|, \end{aligned}$$

Using the definition of the diffusion equation (4), one can obtain a bound for the term $\|\nabla q(x, t)\|_{H^0(V)}$ as

$$\begin{aligned} \|\nabla q(x, t)\|_{H^0(V)} &= \left\| -\beta u_t(x, t) + \sum_{i=1}^n \mathcal{B}_i(x) Q_i(t) \right\|_{H^0(V)} \\ &\leq \beta \|u_t(x, t)\|_{H^0(V)} + \left\| \sum_{i=1}^n \mathcal{B}_i(x) Q_i(t) \right\|_{H^0(V)} \\ &\leq \beta \|u_t(x, t)\|_{H^0(V)} + \sum_{i=1}^n \frac{1}{\sqrt{V_i^*}} |Q_i(t)| \\ &\leq \beta \Gamma_{u_t} + \frac{\sqrt{n}}{\sqrt{V^*}} L_Q, \quad \forall t \in T, \end{aligned} \quad (40)$$

where $\frac{1}{\sqrt{V^*}} = \sum_{i=1}^n \frac{1}{\sqrt{V_i^*}}$ and the bound (30) and Assumption 1 have been used. (37) as

Then, using the previous bound, Assumption 2 and (33), the term $\|\Psi_2(t)\|$ can be upper bounded as

$$\begin{aligned} \|\Psi_2(t)\| &\leq \frac{\sqrt{m_u}}{\beta\sqrt{V_{uT}}} \left(\beta\Gamma_{u_t} + \frac{\sqrt{n}}{\sqrt{V^*}}L_Q \right) + L_{\dot{r}_u} \\ &\quad + \frac{\gamma_1^M \sqrt{m_R}}{\gamma_{10}R^* \beta V_{RT}} \Gamma_R \left(\beta\Gamma_{u_t} + \frac{\sqrt{n}}{\sqrt{V^*}}L_Q \right) \\ &\quad + \frac{\gamma_2^M \sqrt{m_R}}{\gamma_{10}R^* V_{RT}} \Gamma_R^2 \\ &\quad + \frac{\gamma_2^M}{\gamma_{10}} L_{r_R} + \frac{1}{\gamma_{10}R^*} L_{\dot{r}_R} \\ &\leq \Gamma_{\Psi_2} < \infty, \quad \forall t \in T, \end{aligned} \quad (41)$$

for $\Gamma_{\Psi_2} > 0$. A similar procedure can be performed (derivate w.r.t. the time expressions (39) and (40), and use the bounds (33), (34), (31) and Assumptions 1, 2 and 3) to bound $\|\dot{\Psi}_2(t)\|$ as

$$\begin{aligned} \|\dot{\Psi}_2(t)\| &\leq \frac{\sqrt{m_u}}{\beta\sqrt{V_{uT}}} \left(\beta\Gamma_{u_{tt}} + \frac{\sqrt{n}}{\sqrt{V^*}}L_{\dot{Q}} \right) + L_{\dot{r}_u} \\ &\quad + \frac{L_{\gamma_1} \sqrt{m_R}}{\gamma_{10}R^* \beta V_{RT}} \Gamma_R \left(\beta\Gamma_{u_t} + \frac{\sqrt{n}}{\sqrt{V^*}}L_Q \right) \\ &\quad + \frac{\gamma_1^M \sqrt{m_R}}{\gamma_{10}R^* \beta V_{RT}} \Gamma_{R_t} \left(\beta\Gamma_{u_t} + \frac{\sqrt{n}}{\sqrt{V^*}}L_Q \right) \\ &\quad + \frac{\gamma_1^M \sqrt{m_R}}{\gamma_{10}R^* \beta V_{RT}} \Gamma_R \left(\beta\Gamma_{u_{tt}} + \frac{\sqrt{n}}{\sqrt{V^*}}L_{\dot{Q}} \right) \\ &\quad + \frac{L_{\gamma_2} \sqrt{m_R}}{\gamma_{10}R^* V_{RT}} \Gamma_R^2 + \frac{\gamma_2^M \sqrt{m_R}}{\gamma_{10}R^* V_{RT}} \Gamma_R \Gamma_{R_t} \\ &\quad + \frac{\gamma_2^M}{\gamma_{10}} L_{\dot{r}_R} + \frac{1}{\gamma_{10}R^*} L_{\dot{r}_R} \\ &\leq \Gamma_{\dot{\Psi}_2} < \infty, \quad \forall t \in T. \end{aligned} \quad (42)$$

We will obtain a bound over the derivative $\|\dot{\Psi}_2(t)\| = \left\| \frac{d}{dt} \left[\frac{1}{b} [\mathbb{I}_m + \Delta B(t)]^{-1} \Psi_2(t) \right] \right\|$ as follows

$$\begin{aligned} \|\dot{\Psi}_2(t)\| &\leq \frac{1}{b} \left\| (\mathbb{I}_m + \Delta B(t))^{-1} \frac{d}{dt} [\Delta B(t)] (\mathbb{I}_m + \Delta B(t))^{-1} \right\| \\ &\quad \times \|\Psi_2(t)\| + \frac{1}{b} \left\| (\mathbb{I}_m + \Delta B(t))^{-1} \right\| \|\dot{\Psi}_2(t)\| \\ &\leq \frac{1}{b(1-\delta_B)^2} \left\| \frac{d}{dt} [\Delta B(t)] \right\| \Gamma_{\Psi_2} + \frac{1}{b(1-\delta_B)} \Gamma_{\dot{\Psi}_2}, \end{aligned}$$

where the bounds (41) and (42) have been used and the expression $\left\| (\mathbb{I}_m + \Delta B(t))^{-1} \right\| \leq \frac{1}{1-\delta_B}$ has been taken into account, which is valid due to the bound (18), proven in the previous step. Let us calculate the term $\left\| \frac{d}{dt} [\Delta B(t)] \right\|$ using

$$\begin{aligned} \left\| \frac{d}{dt} [\Delta B(t)] \right\| &\leq \max_{i=1, \dots, m_R} \left\{ \frac{\beta_0}{\beta\gamma_{10}R^*V_{R_i^*}} \int_{V_{R_i^*}} \dot{\gamma}_1(x, t) R(x, t) dV \right. \\ &\quad \left. + \frac{\beta_0}{\beta\gamma_{10}R^*V_{R_i^*}} \int_{V_{R_i^*}} \dot{\gamma}_1(x, t) R_t(x, t) dV \right\} \\ &\leq \max_{i=1, \dots, m_R} \left\{ \frac{\beta_0}{\beta\gamma_{10}R^* \sqrt{V_{R_i^*}}} \right\} \\ &\quad \times \left(L_{\dot{\gamma}_1} \|R(x, t)\|_{H^0(V)} + \gamma_1^M \|R_t(x, t)\|_{H^0(V)} \right) \\ &\leq \rho_1 L_{\dot{\gamma}_1} \Gamma_R + \rho_1 \gamma_1^M \Gamma_{R_t}, \quad \forall t \in T, \end{aligned}$$

where $\rho_1 = \max_{i=1, \dots, m_R} \left\{ \frac{\beta_0}{\beta\gamma_{10}R^* \sqrt{V_{R_i^*}}} \right\}$ and the bounds (33), (34), and Assumption 3 have been used. Finally, the term $\|\dot{\Psi}_2(t)\|$ can be bounded as

$$\begin{aligned} \|\dot{\Psi}_2(t)\| &\leq \frac{\rho_1}{b(1-\delta_B)^2} \Gamma_{\Psi_2} (L_{\dot{\gamma}_1} \Gamma_R + \gamma_1^M \Gamma_{R_t}) \\ &\quad + \frac{1}{b(1-\delta_B)} \Gamma_{\dot{\Psi}_2} \\ &\leq \rho_2 < \infty, \quad \forall t \in T, \end{aligned}$$

for some $\rho_2 > 0$. This term is also bounded as in (21) with $\delta_3 \geq \rho_2$ and any $\delta_4 > 0$. \square

These four steps conclude the proof. \blacksquare

Remark 3: As a consequence of the stability of the closed-loop system (23), the integral term, ν , of the control (16) is able to provide an estimate of the perturbation $\bar{\Psi}_2(t)$ in finite-time, i.e., $\nu(t) = -\frac{1}{b} [\mathbb{I}_m + \Delta B(t)]^{-1} \Psi_2(t)$ after a finite-time.

Remark 4: Theorem 1 can be also obtained for Dirichlet BCs in the diffusion equation (4), i.e., $u(x, t) = 0$ for all $x \in S$. On that case, the change of coordinates (24) is not necessary and Lyapunov functionals $\mathcal{V} = \frac{1}{2} \|\cdot\|_{H^0(V)}^2$, for $u(x, t), u_t(x, t), u_{tt}(x, t)$, can be used to retrieve the eISS bounds

$$\|u(x, t)\|_{H^0(V)} \leq \|u(x, 0)\|_{H^0(V)} + \frac{\epsilon\eta^M \sqrt{n}}{k^m \sqrt{V_T^*}} L_Q,$$

$$\|u_t(x, t)\|_{H^0(V)} \leq \frac{\epsilon\eta^M \sqrt{n}}{k^m \sqrt{V_T^*}} L_{\dot{Q}} \leq \Gamma_{u_t},$$

$$\|u_{tt}(x, t)\|_{H^0(V)} \leq \frac{\epsilon\eta^M \sqrt{n}}{k^m \sqrt{V_T^*}} L_{\dot{Q}} \leq \Gamma_{u_{tt}}, \quad \forall t \in T. \quad (43)$$

The rest of the proof remains the same.

A. Demand and input constraints

Following [34], we will consider a new feature where an additional number of flux restrictions, n_r , with $n_r + m \leq n$, over the inputs $Q(t)$ of system (4) is needed. In other words, we will impose the weighted sum of the injection rates of some of the inputs to be equal to a time-variant function.

The condition imposed over the control input, $Q(t)$, is

$$WQ(t) = D(t), \quad (44)$$

where $W \in \mathbb{R}^{n_r \times n}$ is a full rank matrix whose elements represent the weighted participation of the input fluxes for ensuring the demand $D(t) \in \mathbb{R}^{n_r}$. In order to follow this, the control input will be designed as

$$\begin{aligned} Q(t) &= \overline{W} (B_0 \overline{W})^+ [-k_1 \phi_1(\sigma(t)) + b\nu(t)] \\ &\quad + W^T (WW^T)^{-1} D(t), \\ \dot{\nu}(t) &= -k_2 \phi_2(\sigma(t)), \end{aligned} \quad (45)$$

where $\sigma(t)$ is the original error vector, $\phi_1(\sigma(t)), \phi_2(\sigma(t))$ are defined in (17), and $\overline{W} \in \mathbb{R}^{n \times (n-n_r)}$ is the null space of W . Note that if we replace (45) in (44), the demand over the controlled injection points will be strictly fulfilled at any time $t \in T$.

Control (45) will ensure the linear combination of the input $Q(t)$ to be equal to a predetermined flux $D(t)$, which we called demand, according to (44). This new addition does not change the original output tracking result and it will be used for the case study of the next Section.

IV. PREVENTION OF INDUCED SEISMICITY IN GRONINGEN RESERVOIR

The Groningen gas field, located at the northeastern Netherlands, is one of the largest natural gas fields in both Europe and the world, with an estimated 2,900 billion cubic meters of recoverable gas. However, gas extraction in Groningen triggered earthquakes since 1991, which caused damage to buildings and concern among residents. In June 2023, the Dutch government announced that gas extraction would end by October 1, 2023, leaving about 470 billion cubic meters of gas still in the field [20], [21].

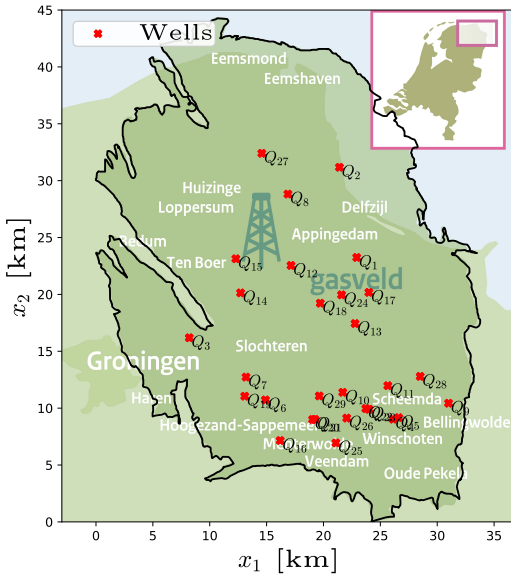


Fig. 1. Groningen gas reservoir. Background image was obtained from the public image <https://zoek.officiëlebezoekmakingen.nl/stcrt-2017-28922.html>.

Injection and extraction of fluids at depth cause fluid circulation within the reservoir, leading to deformation of the surrounding porous rock. This hydro-mechanical behaviour

can be described by Biot's theory [40], which couples fluid diffusion and rock deformation. However, when fluid injection rates are slow and rock volumetric strain is negligible, the diffusion of the fluid in the host rock due to fluid injections/extractions can be described by the diffusion equation in (4) (see [41], [42]), where $u(x, t)$ is the change of the fluid pressure in the reservoir due to fluid injections, $x \in V$ is the spatial coordinate, $t \in T$ is the time, $q(x, t)$ is the change of the hydraulic flux and $B_i(x)Q_i(t)$, $i = 1, \dots, n$, are source/sink terms representing the fluid injections/extractions, as defined in the previous section. In Groningen, $n = 29$ wells are located along the reservoir (see Fig. 1). $k(x, t)$ is the permeability matrix of the host rock, $\eta(x, t)$ is the dynamic viscosity of the fluid, and β is the compressibility of the rock-fluid mixture. The reservoir has a volume V , and undrained boundary conditions were considered at the boundary of the reservoir, *i.e.*, $q(x, t) \cdot \hat{e} = 0$ at $S = \partial V$ (see [43], [44], [45], [46], [47] for more details of the BCs in Groningen).

It is well established that fluid injection and extraction can activate or create seismic faults, leading to significant earthquakes. This seismicity is related to stress changes in the rocks caused by fluid movement, which increases the likelihood of fault slip and intensifies seismic activity (as discussed in [12], [17], [48] in general, and in [43], [44], [45] in the particular case of Groningen). In other words, fluid injections/extractions increase the seismicity rate (SR) in a region, *i.e.*, the number of earthquakes (events) in a given time window.

The seismicity rate can be modelled with system (6), where $R(x, t)$ denotes the point-wise SR density, $u_t(x, t)$ is the input of this system and denotes the partial derivative of $u(x, t)$ with respect to time, $\gamma_1(x, t)$ represents the inverse of the background stress change, *i.e.* the stress change due to various natural tectonic processes, and $\gamma_2(x, t)$ the inverse of the characteristic number of events. Such equation coincides with the one of Segall and Lu [49] (see also [50]), and it is defined point-wise, differently from [34] where the SR is defined region-wise.

In the absence of fluid injections, $u_t(x, t) = 0$ and, therefore, $R(x, t) \rightarrow R^*$. In this case, the SR of the region reduces to the natural one. If, on the contrary, fluids are extracted from the reservoir, then $\dot{u} < 0$ leading to an increase of the SR ($\dot{R}(x, t) > 0$). This is demonstrated from real data and modelling of the reservoir (see [20], [21], [43], [44], [45], [51], [46], [47]), between 10-1965 to 01-2023. Fig. 2 shows the total gas extraction history ($-\sum_{i=1}^{29} Q_i(t)$) in the whole reservoir. The distribution of all the events during the total period is shown in the left side of Fig. 3. Fig. 4 (blue line) shows the average SR over the whole reservoir ($\bar{R}(x, t)$) and the cumulative number of events ($\int_T \bar{R}(x, t) dt$). 712 seismic events were registered in total from 12-1991 to 01-2023.

Gas extraction has caused earthquakes in the Groningen reservoir, leading to its closure. In this paper, we will use the designed control (16) to avoid induced seismicity while keeping the same extraction of gas, starting from 12-1991. For that purpose, we will first select parameters and coefficients for systems (4)–(6) to fit and validate the model against real reservoir data.

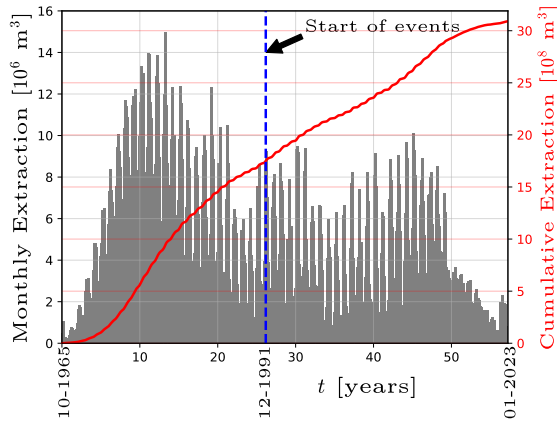


Fig. 2. Monthly and cumulative extraction of gas in Groningen.

TABLE I

DIFFUSION AND SEISMICITY RATE SYSTEM PARAMETERS.

Parameter	Description	Value and Units
c_{hy}	Hydraulic diffusivity	$4.4 \times 10^{-2} \mathbb{I}_3$ [km ² /hr]
β	Mixture compressibility	5.7×10^{-4} [1/MPa]
γ_1^M	Inverse of maximum background stress change	4.7 [1/MPa]
γ_2	Inverse of characteristic number of events	1.08×10^{-2} [1/events]
R^*	Background SR	0.99 [events/year]

A. Model setup and validation

We start by selecting the parameters of system (4). We consider the parameters of Table I according to [43], [44], [45], [46], [47], where $c_{hy} = k(x,t)/\beta\eta(x,t)$ results to be a constant value. Then, we check that the average pressure over the reservoir fits the one shown in [44, Figure 1]. For that purpose, we depth average Equation 4 and we integrate the resulting partial differential equation in time and space using a finite elements as explained in Appendix I. The extraction of wells $Q_i(t)$ was selected from real extraction history reported in [20], [21], [51].

The result is shown in Fig. 5 where similar results were obtained to the ones reported in [44, Figure 1] using more detailed models for the Groningen reservoir.

For the validation of system (4), an optimization algorithm was implemented to select $\gamma_1(x,t), \gamma_2(x,t)$ based on the normalized spatial density of the real SR data shown in Fig. 3 (left side). The normalized simulated density, $d(x)$, is shown in Fig 3 (right side). The optimized parameters are written in Table I, where $\gamma_1(x,t) = \gamma_1(x) = \gamma_1^M d(x)$ and $\gamma_2(x,t) = \gamma_2$. Notice that these parameters are consistent with the more sophisticated models and studies performed in [43], [44], [45], [46], [47]. Furthermore, the average SR and the cumulative number events obtained from our model match quite well the real data for the needs of the present example (Fig. 4). Finally, the norms of $u(x,t)$ and $R(x,t)$ are shown in Fig. 6, which will be useful for the control gains selection.

Two control scenarios will be explored, starting from the date when seismic events began in 12-1991. In the first scenario, we will apply control (45) to regulate the average pressure across five regions of the reservoir ($V_{u_i}, i = 1, \dots, 5$)

and manage the average SR in the remainder of the reservoir (V_{R_1}), all while maintaining the same fluid extraction profile as shown in Fig. 2. This extraction profile will serve as the demand, $D(t)$. The selection of these five regions is based on the locations of major towns in the Groningen area (see Fig. 1) and is illustrated in Fig. 7. In the second scenario, we will introduce an additional constraint on the input $Q(t)$ by incorporating CO₂ injection. This scenario aims to maintain a zero net impact from CO₂, resulting in a green method for energy generation.

B. Scenario 1: Gas extraction

The control (17), (45) was implemented with a demand $D(t) = -f(t)$, where $f(t)$ is the extraction history shown in Fig. 2, noting that extraction is represented by a negative sign. The weight matrix, $W \in \mathbb{R}^{1 \times 29}$, was selected as a full matrix filled with random numbers between 0.8 and 1.2. The error vector was implemented as in (7), (10), with $\gamma_{1_0} = 3.93 \times 10^7$, according to condition (38) (Γ_R was chosen as the highest value from Fig. 6 and $V_{R_i}^*$ was selected as the smallest volume in the discretization).

The pressure references were chosen ad-hoc to guide the outputs to an average pressure after 15 [years] using a sigmoid profile, while the SR reference was maintained at R^* . The control gains were designed according to (22), (38), with $l = 1 \times 10^{-4}$, $\bar{k}_2 = 1 \times 10^4$, $b = 1$, and $\Gamma_R, V_{R_i}^*$ as selected before, resulting in $k_1 = 2.22 \times 10^{-2}$, $k_2 = 1 \times 10^{-4}$, $\alpha_1 = 0.3$, and $\alpha_2 = 80$. The nominal matrix B_0 was selected as in (15), with $\beta_0 = 0.8\beta$, in accordance with condition (38).

The results are displayed in Figs. 8 and 9. The control successfully drives all the pressure outputs to their smooth references. The average SR presents an overshoot in the beginning but then it remains close to the reference R^* . Therefore, the control prevents new seismic events throughout region V_{R_1} , in contrast with the real, uncontrolled scenario shown in Fig. 4. Additionally, this was achieved while satisfying exactly the total gas extraction demand, as shown in Fig. 9. The control signal stays within acceptable saturation levels for realistic wells, and the observed oscillations are due to the demand signal rather than the control definition.

C. Scenario 2: Gas extraction and CO₂ injection

The same gains and parameters as in Scenario 1 were used in this case too, with the exception of the demand and weight matrix. To achieve a zero net impact, the same mass of CO₂ must be injected as the mass of the potential C₂ emissions of the extracted gas. This is accomplished by injecting approximately 1.36 times the gas demand, based on the reservoir conditions (60 [MPa] of pressure at 100 [°C] at the injection depth). Consequently, the demand is set to $D(t) = [-f(t), 1.36f(t)]$ and the weight matrix $W \in \mathbb{R}^{2 \times 29}$ is defined ad-hoc such that its first row assigns random numbers (between 0.8 and 1.2) to the first 14 elements of $Q(t)$, and its second row assigns random numbers (between 0.8 and 1.2) to the last 15 elements.

The results are shown in Figs. 10 and 11. The control successfully drives both types of outputs (pressure and SR)

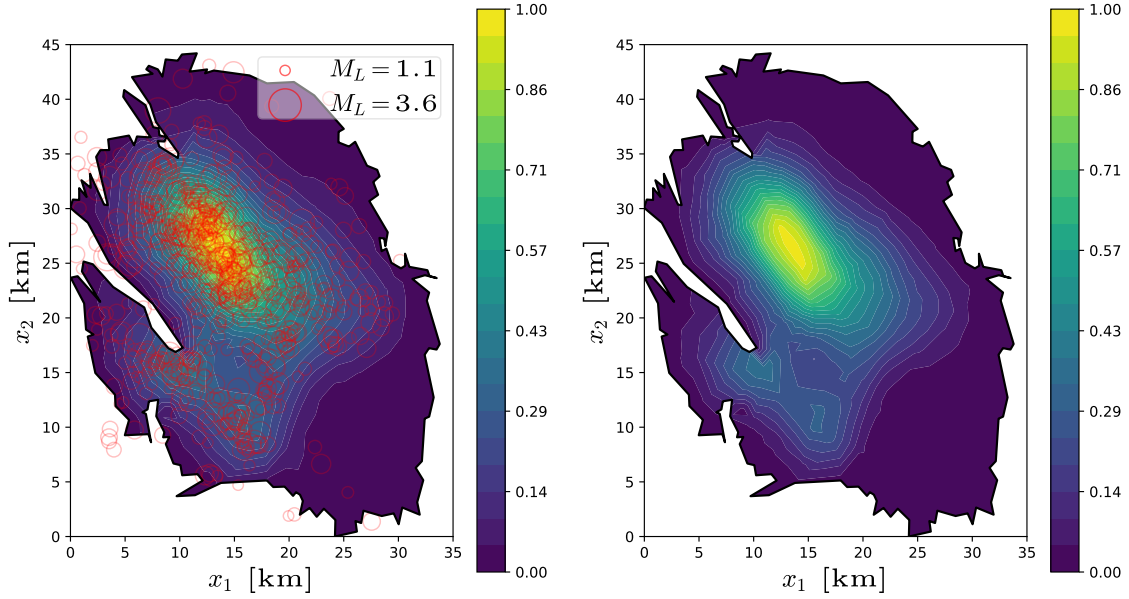


Fig. 3. Normalized spatial density map of the SR in Groningen representing the 712 events that occurred between 12-1991 and 01-2023. Left image shows the magnitude and location of the real seismic events, from which their spatial density is determined. The right image depicts the simulated spatial density of the events. The normalization was made with the maximum value of the spatial density of $R(x, t)$ over the reservoir.

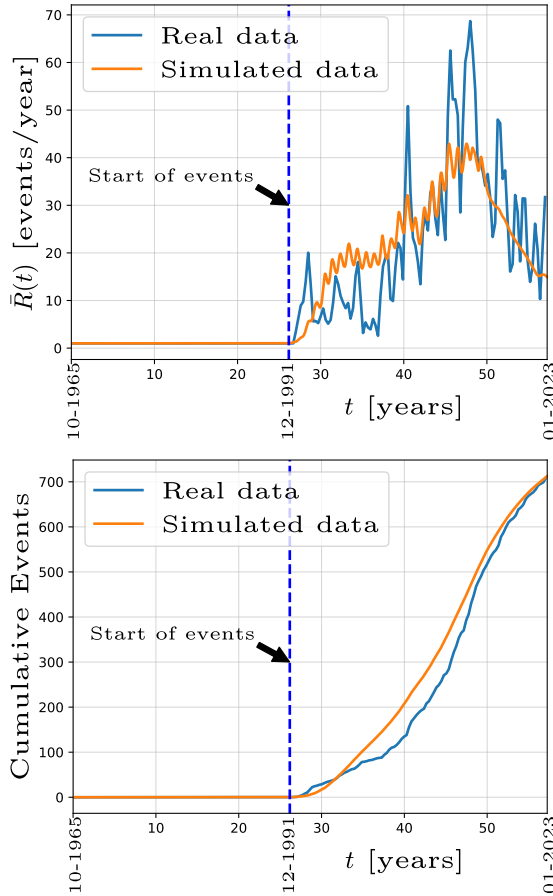


Fig. 4. Average SR over the reservoir and cumulative number of seismic events in Groningen. Real data (blue line) and simulated data (orange line).

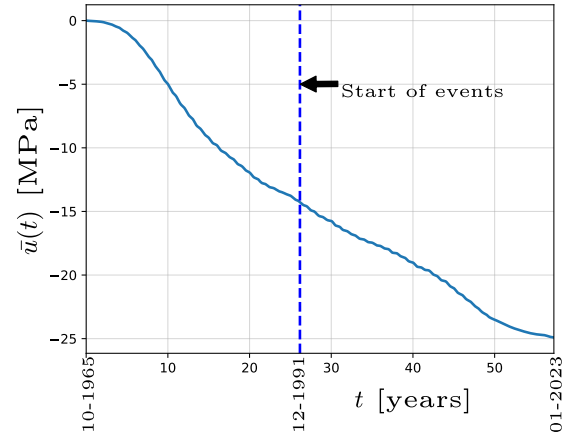


Fig. 5. Average pressure over the reservoir (see also [44, Figure 1]).

to their respective references. In this case, the SR is even closer to its reference compared to scenario 1. The generated control signal exhibits lower saturation levels than in scenario 1, resulting in less energy being required to achieve zero net impact. Lastly, both types of demands (injection and extraction) are followed at each time step.

D. Comparison and limitations

The results of both scenarios will be compared. First, the norm of the error is shown in Fig. 12. In both scenarios, the control strategy successfully stabilizes the error norm in finite time, as expected, achieving the same level of precision. Therefore, overshoot and oscillations present in the SR error of Fig. 8 could be improved by another selection of the parameter γ_{10} , as seen in (10). Second, Fig. 13 illustrates the cumulative number of events over the entire simulation

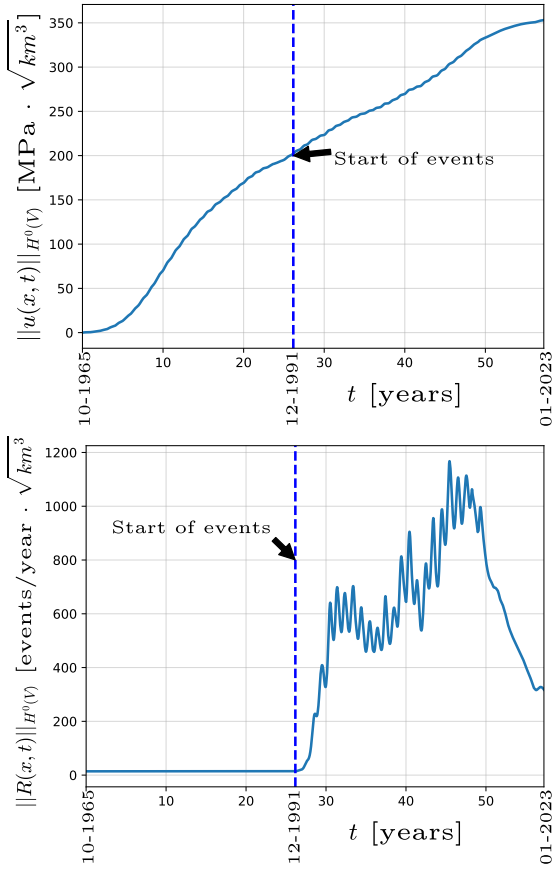


Fig. 6. Norms of $u(x, t)$ (top) and $R(x, t)$ (bottom) in the simulation.

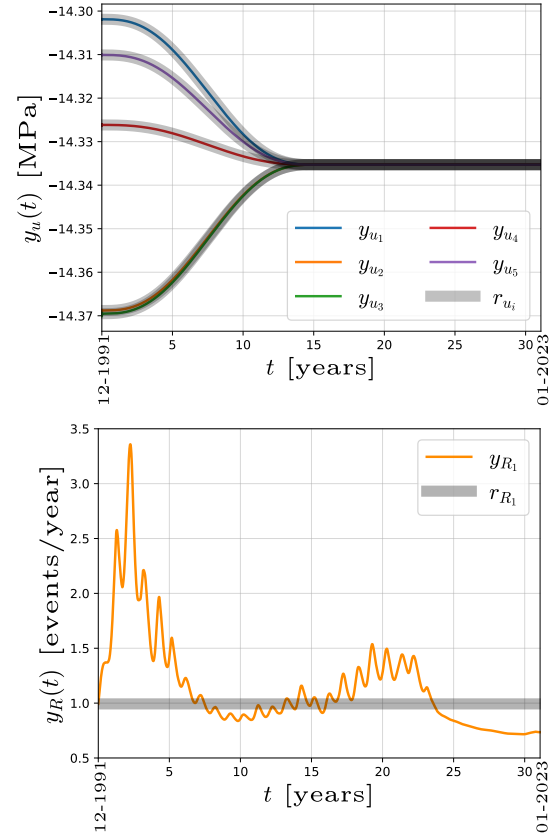


Fig. 8. Pressure (top) and SR (bottom) outputs in Scenario 1.

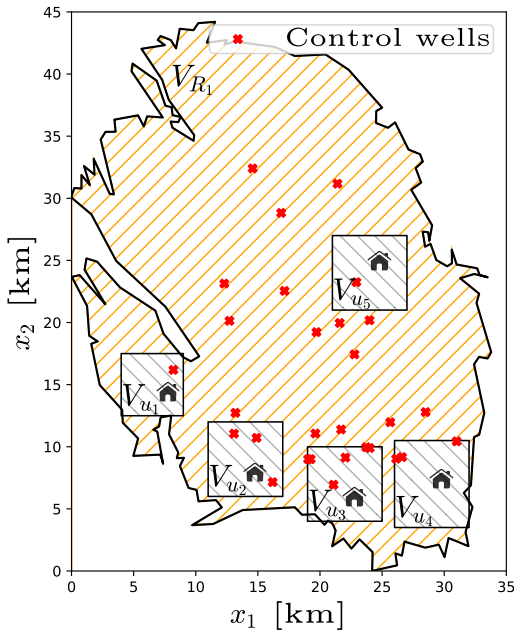


Fig. 7. Groningen reservoir with regions for controlling pressure and SR based on the locations of major towns in the area.

period (≈ 31 [years]), compared to the case without extraction, where the background SR predicts the cumulative events as $\int_0^t R^* dt = R^*t$. The background SR is assumed to be equal

to the fitted one, starting in 1991 (see Table I). The final value in this case is approximately 31 [events]. Scenario 1 results in a total of 35 [events], only four more than the case without extraction. On the other hand, Scenario 2 follows the same trajectory as the no-extraction case, indicating that no additional seismic events are generated during the injection and extraction processes. This demonstrates that the proposed control strategy effectively prevents induced seismicity, significantly reducing the 712 [events] for the case without control (see Fig. 4). Finally, Fig. 14 displays the norm of the solution for both $u(x, t)$ and $R(x, t)$. Scenario 1 shows a higher norm in both cases, but both scenarios significantly reduce the norms compared to the reference simulation without control shown in Fig. 6.

However, evaluating earthquake risk based solely on the seismicity rate has its limitations, as earthquake magnitude is often more critical than the rate of seismic activity. The relationship between earthquake magnitude and frequency can be described by a modified Gutenberg-Richter distribution, as discussed in [52], [46]. However, incorporating stochasticity exceeds the scope of this work.

Additionally, the inclusion of fault discontinuities needs to be addressed in real-world applications. Managing multiple faults within a reservoir (*cf.*, [53]) is particularly challenging due to the complexity and multiphase flow, as well as the rapid spatio-temporal scales linked to poroelastodynamic processes triggered by intermittent fluid injections. Poroelastodynamic phenomena were ignored on this work and are currently under

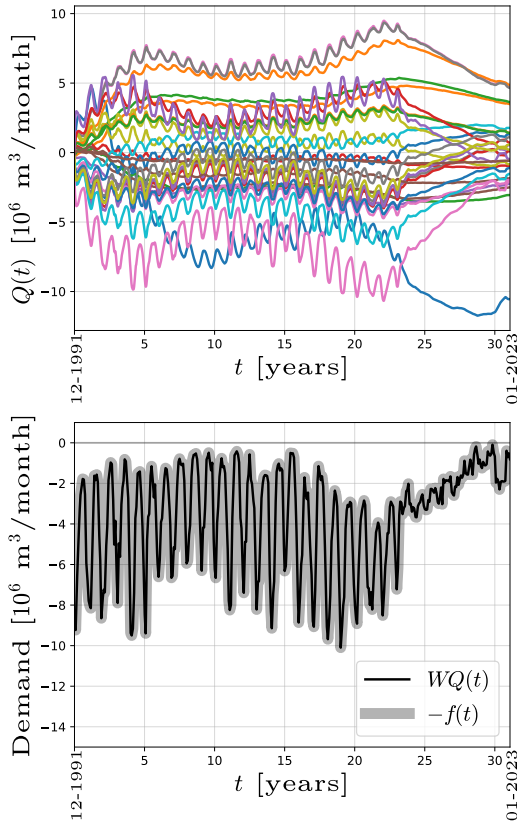


Fig. 9. Control signals (top) and demand (bottom) in Scenario 1.

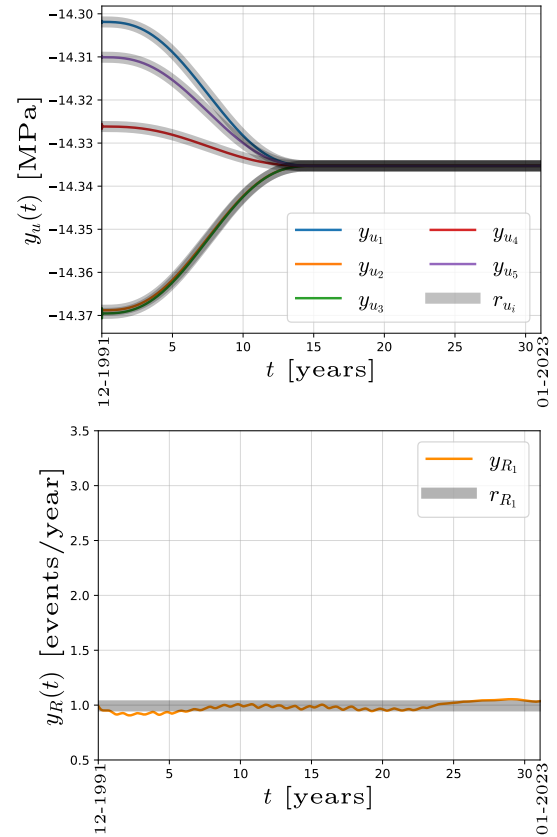


Fig. 10. Pressure (top) and SR (bottom) outputs in Scenario 2.

investigation.

Finally, control signals like those shown in Figs. 9 and 11 might be unfeasible in real wells because of the sign reversal, the technical characteristic of the pumps and wells' integrity (saturation of the control input). These phenomena, together with other technoeconomical limitations require specific attention and will be addressed in the future in specific case studies.

V. CONCLUSION

This paper introduces a robust control strategy for output tracking of a nonlinear 3D PDE-ODE system. The output feedback control was developed through a rigorous mathematical analysis of the cascade system, which was divided into parts: first, the bounds for the solution and its time derivative in both the infinite-dimensional system and the nonlinear ODE were obtained; then, these bounds were used to prove the boundedness of the uncertain control coefficient and the perturbation in the error dynamics. The mathematical formulation demonstrates the controller's capability to manage tracking for two types of outputs in the system, even in the presence of heterogeneities in the system, model uncertainties, and under limited system information, all while using a continuous control signal.

A case study focused on preventing induced seismicity while ensuring energy production in the Groningen gas reservoir is presented to validate the control method. Unlike existing methods for mitigating induced seismicity caused

by fluid injections in the Earth's crust, the proposed control approach ensures robust tracking of desired seismicity rates and pressures across selected regions of the geological reservoir, despite the presence of uncertainties. This is particularly valuable in such complex systems, where real parameters (such as diffusivity and compressibility) are often difficult to acquire accurately. Moreover, the control design effectively addressed the complex interconnection between the infinite-dimensional system and the nonlinear ODE in three dimensions.

Numerical simulations illustrate that our control approach not only enables the extraction of the same quantity of gas from the Groningen reservoir with minimal seismicity, but also demonstrates how parallel CO₂ injections could achieve a neutral environmental impact. While our theoretical approach has limitations, robust control theory offers new possibilities for addressing the challenges of uncertain, nonlinear distributed parameter systems providing a framework for balancing the prevention of induced seismicity with the optimization of renewable energy production and storage.

The integration of more realistic scenarios, such as the presence of multiple faults, poroelastodynamic processes, and the inclusion of saturation limits in the control inputs, remains an open problem and is a key focus for future research.

- [1] H. Khalil, *Nonlinear Systems*. New Jersey, U.S.A.: Prentice Hall, 2002.
- [2] L. C. Evans, *Partial differential equations*. Rhode Island, USA: American Mathematical Society, 2010.

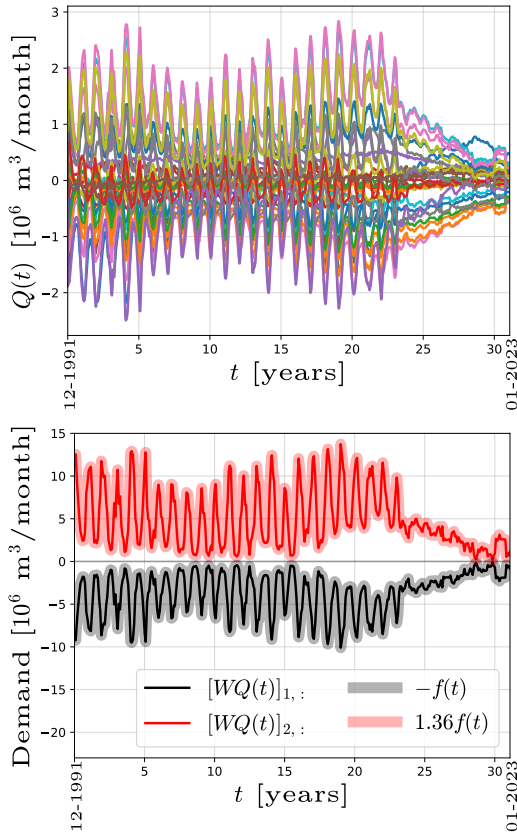


Fig. 11. Control signals (top) and demand (bottom) in Scenario 2.

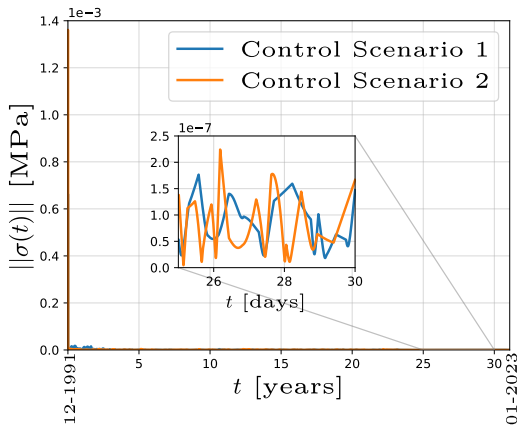


Fig. 12. Error norm in both scenarios.

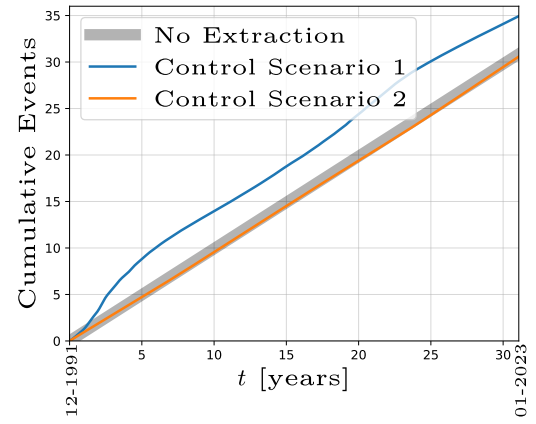


Fig. 13. Total cumulative events in both scenarios.

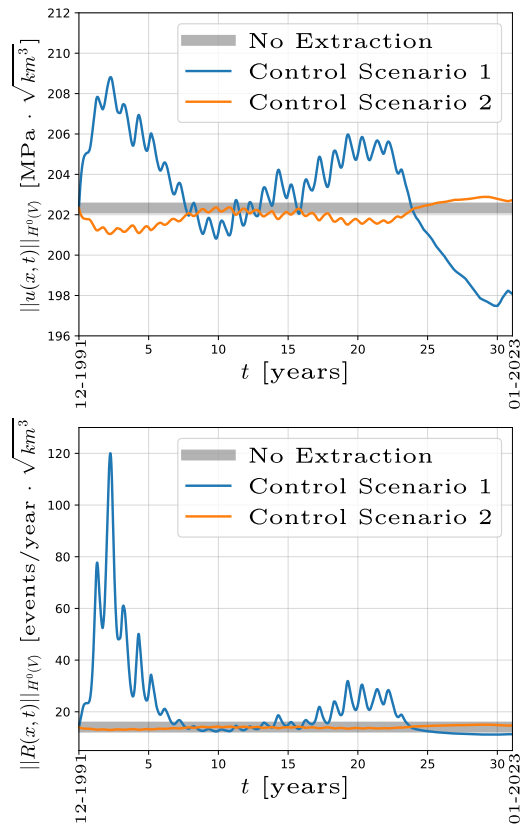


Fig. 14. Norms of $u(x, t)$ (top) and $R(x, t)$ (bottom) in both scenarios.

[3] J. Zhong, S. Liang, Y. Yuan, and Q. Xiong, "Coupled electromagnetic and heat transfer ode model for microwave heating with temperature-dependent permittivity," *IEEE Transactions on Microwave Theory and Techniques*, vol. 64, no. 8, pp. 2467–2477, 2016.

[4] S. Koch, A. Piloni, A. Pisano, and E. Usai, "Sliding-Mode Boundary Control of an In-Line Heating System Governed by Coupled PDE/ODE Dynamics," *IEEE Transactions on Control Systems Technology*, vol. 30, no. 6, pp. 2689–2697, 2022.

[5] A. Quarteroni and A. Veneziani, "Analysis of a geometrical multiscale model based on the coupling of ODE and PDE for blood flow simulations," *Multiscale Modeling & Simulation*, vol. 1, no. 2, pp. 173–195, 2003.

[6] J. Deutscher and N. Gehring, "Output Feedback Control of Coupled Linear Parabolic ODE–PDE–ODE Systems," *IEEE Transactions on Automatic Control*, vol. 66, no. 10, pp. 4668–4683, 2020.

[7] S. Tang and C. Xie, "State and output feedback boundary control for a coupled PDE–ODE system," *Systems & Control Letters*, vol. 60, no. 8, pp. 540–545, 2011.

[8] D. Zhao, B. Jiang, and H. Yang, "Backstepping-based decentralized fault-tolerant control of hypersonic vehicles in PDE–ODE form," *IEEE Transactions on Automatic Control*, vol. 67, no. 3, pp. 1210–1225, 2021.

[9] G. A. Susto and M. Krstic, "Control of PDE–ODE cascades with Neumann interconnections," *Journal of the Franklin Institute*, vol. 347, no. 1, pp. 284–314, 2010.

[10] J.-M. Wang, J.-J. Liu, B. Ren, and J. Chen, "Sliding mode control to stabilization of cascaded heat PDE–ODE systems subject to boundary control matched disturbance," *Automatica*, vol. 52, pp. 23–34, 2015.

[11] M. P. Wilson, G. R. Foulger, J. G. Gluyas, R. J. Davies, and B. R. Julian, "HiQuake: The Human-Induced Earthquake Database," *Seismological Research Letters*, vol. 88, pp. 1560–1565, 10 2017.

[12] J. L. Rubinstein and A. B. Mahani, "Myths and facts on wastewater

- injection, hydraulic fracturing, enhanced oil recovery, and induced seismicity," *Seismological Research Letters*, vol. 86, no. 4, pp. 1060–1067, 2015.
- [13] F. Grigoli, S. Cesca, E. Priolo, A. P. Rinaldi, J. F. Clinton, T. A. Stabile, B. Dost, M. G. Fernandez, S. Wiemer, and T. Dahm, "Current challenges in monitoring, discrimination, and management of induced seismicity related to underground industrial activities: A european perspective," *Reviews of Geophysics*, vol. 55, no. 2, pp. 310–340, 2017.
- [14] M. Maheux, "Géothermie : "Dans le Bas-Rhin, tous les projets sont à l'arrêt" annonce la préfète," *France Bleu*, 9/12/2020. . Available at: <https://www.francebleu.fr/infos/societe/geothermie-profonde-tous-les-projets-sont-a-l-arret-declare-la-prefete-du-bas-rhin-1607534951>.
- [15] N. Stey, "En Alsace, les projets de géothermie profonde à l'arrêt," *Le Monde*, 11/12/2020. . Available at: https://www.lemonde.fr/planete/article/2020/12/11/en-alsace-les-projets-de-geothermie-profonde-a-l-arret_6063099_3244.html.
- [16] K. Dae-sun, "Findings of Pohang earthquake causes halt energy project on Ulleung Island," *Hankyoreh english*, 24/03/2019. . Available at: https://www.hani.co.kr/arti/english_edition/e_national/887126.html.
- [17] M. Zastrow, "South Korea accepts geothermal plant probably caused destructive quake," *Nature*, 2019.
- [18] N. Deichmann and D. Giardini, "Earthquakes Induced by the Stimulation of an Enhanced Geothermal System below Basel (Switzerland)," *Seismological Research Letters*, vol. 80, pp. 784–798, 09 2009.
- [19] J. Glanz, "Quake Threat Leads Swiss to Close Geothermal Project," *New York Times*, 10/12/2009. . Available at: <https://www.nytimes.com/2009/12/11/science/earth/11basel.html#:~:text=A%20%2460%20million%20project%20to,project%2C%20led%20by%20Markus%20>.
- [20] T. N. D. Oil and G. Portal, "Groningen gas field," 2023. <https://www.nlog.nl/groningen-gasveld>.
- [21] Rijksoverheid, "Dashboard Groningen," 2023. <https://dashboardgroningen.nl>.
- [22] J. P. Verdon and J. J. Bommer, "Green, yellow, red, or out of the blue? An assessment of Traffic Light Schemes to mitigate the impact of hydraulic fracturing-induced seismicity," *Journal of Seismology*, vol. 25, pp. 301–326, 2021.
- [23] H. Hofmann, G. Zimmermann, M. Farkas, E. Huenges, A. Zang, M. Leonhardt, G. Kwiatek, P. Martinez-Garzon, M. Bohnhoff, K.-B. Min, P. Fokker, R. Westaway, F. Bethmann, P. Meier, K. S. Yoon, J. W. Choi, T. J. Lee, and K. Y. Kim, "First field application of cyclic soft stimulation at the Pohang Enhanced Geothermal System site in Korea," *Geophysical Journal International*, vol. 217, no. 2, pp. 926–949, 2019.
- [24] L. P. Frash, P. Fu, J. Morris, M. Gutierrez, G. Neupane, J. Hampton, N. J. Welch, J. W. Carey, and T. Kneafsey, "Fracture caging to limit induced seismicity," *Geophysical Research Letters*, vol. 48, no. 1, p. e2020GL090648, 2021.
- [25] A. Zang, G. Zimmermann, H. Hofmann, O. Stephansson, K.-B. Min, and K. Y. Kim, "How to Reduce Fluid-Injection-Induced Seismicity," *Rock Mechanics and Rock Engineering*, vol. 52, pp. 475–493, 2019.
- [26] S. Baisch, C. Koch, and A. Muntendam-Bos, "Traffic Light Systems: To What Extent Can Induced Seismicity Be Controlled?," *Seismological Research Letters*, vol. 90, no. 3, pp. 1145–1154, 2019.
- [27] Y. Ji, W. Zhang, H. Hofmann, Y. Chen, C. Kluge, A. Zang, and G. Zimmermann, "Modelling of fluid pressure migration in a pressure sensitive fault zone subject to cyclic injection and implications for injection-induced seismicity," *Geophysical Journal International*, vol. 232, no. 3, pp. 1655–1667, 2022.
- [28] I. Stefanou, "Controlling anthropogenic and natural seismicity: Insights from active stabilization of the spring-slider model," *Journal of Geophysical Research: Solid Earth*, vol. 124, no. 8, pp. 8786–8802, 2019.
- [29] I. Stefanou and G. Tzortzopoulos, "Preventing instabilities and inducing controlled, slow-slip in frictionally unstable systems," *Journal of Geophysical Research: Solid Earth*, vol. 127, no. 7, p. e2021JB023410, 2022.
- [30] D. Gutiérrez-Oribio, G. Tzortzopoulos, I. Stefanou, and F. Plestan, "Earthquake Control: An Emerging Application for Robust Control. Theory and Experimental Tests," *IEEE Transactions on Control Systems Technology*, vol. 31, no. 4, pp. 1747–1761, 2023.
- [31] D. Gutiérrez-Oribio, Y. Orlov, I. Stefanou, and F. Plestan, "Robust Boundary Tracking Control of Wave PDE: Insight on Forcing Slow-Aseismic Response," *Systems & Control Letters*, vol. 178, p. 105571, 2023.
- [32] D. Gutiérrez-Oribio, I. Stefanou, and F. Plestan, "Passivity-based control of underactuated mechanical systems with coulomb friction: Application to earthquake prevention," *Automatica*, vol. 165, no. 111661, 2024.
- [33] D. Gutiérrez-Oribio, Y. Orlov, I. Stefanou, and F. Plestan, "Advances in Sliding Mode Control of Earthquakes via Boundary Tracking of Wave and Heat PDEs," in *16th International Workshop on Variable Structure Systems and Sliding Mode Control*, (Rio de Janeiro, Brasil), 2022.
- [34] D. Gutiérrez-Oribio and I. Stefanou, "Insights of using control theory for minimizing induced seismicity in underground reservoirs," *Geomechanics for Energy and the Environment*, p. 100570, 2024.
- [35] J. A. Moreno, H. Ríos, L. Ovalle, and L. Fridman, "Multivariable super-twisting algorithm for systems with uncertain input matrix and perturbations," *IEEE Transactions on Automatic Control*, vol. 67, no. 12, pp. 6716–6722, 2022.
- [36] M. A. Estrada, L. Fridman, and J. A. Moreno, "Passive fault-tolerant control via sliding-mode-based lyapunov redesign," *IEEE Transactions on Automatic Control*, pp. 1–11, 2024.
- [37] A. Filippov, *Differential Equations with Discontinuous Right-hand Sides*. Dordrecht, The Netherlands: Kluwer Academic Publishers, 1988.
- [38] Y. Orlov, *Nonsmooth Lyapunov Analysis in Finite and Infinite Dimensions*. Cham, Switzerland: Springer International Publishing, 2020.
- [39] S. Dashkovskiy and A. Mironchenko, "Input-to-state stability of infinite-dimensional control systems," *Math. Control Signals Syst.*, vol. 25, pp. 1–35, 2013.
- [40] M. A. Biot, "General theory of three-dimensional consolidation," *Journal of Applied Physics*, vol. 12, no. 155, pp. 155–164, 1941.
- [41] O. C. Zienkiewicz, C. T. Chang, and P. Bettess, "Drained, undrained, consolidating and dynamic behaviour assumptions in soils," *Geotechnique*, vol. 30, no. 4, pp. 385–395, 1980.
- [42] L. Bagur, *Modeling fluid injection effects in dynamic fault rupture using Fast Boundary Element Methods*. Phd thesis, Institut Polytechnique de Paris, July 2024.
- [43] J. D. Smith, E. R. Heimisson, S. J. Bourne, and J.-P. Avouac, "Stress-based forecasting of induced seismicity with instantaneous earthquake failure functions: Applications to the Groningen gas reservoir," *Earth and Planetary Science Letters*, vol. 594, p. 117697, 2022.
- [44] M. Acosta, J.-P. Avouac, J. D. Smith, K. Sironattanakul, H. Kaveh, and S. J. Bourne, "Earthquake Nucleation Characteristics Revealed by Seismicity Response to Seasonal Stress Variations Induced by Gas Production at Groningen," *Geophysical Research Letters*, vol. 50, no. 19, p. e2023GL105455, 2023.
- [45] H. Kaveh, P. Battle, M. Acosta, P. Kulkarni, S. J. Bourne, and J. P. Avouac, "Induced seismicity forecasting with uncertainty quantification: Application to the groningen gas field," *Seismological Research Letters*, vol. 95, pp. 773–790, 12 2023.
- [46] Y. Tamama, M. Acosta, S. J. Bourne, and J. P. Avouac, "Earthquake growth inhibited at higher coulomb stress change rate at groningen," *Geophysical Research Letters*, vol. 51, no. 20, p. e2024GL110139, 2024.
- [47] S. J. Bourne and S. J. Oates, "Stress-dependent magnitudes of induced earthquakes in the groningen gas field," *Journal of Geophysical Research: Solid Earth*, vol. 125, no. 11, p. e2020JB020013, 2020.
- [48] K. M. Keranen, H. M. Savage, G. A. Abers, and E. S. Cochran, "Potentially induced earthquakes in Oklahoma, USA: Links between wastewater injection and the 2011 Mw 5.7 earthquake sequence," *Geology*, vol. 41, no. 6, pp. 1060–1067, 2013.
- [49] P. Segall and S. Lu, "Injection-induced seismicity: Poroelastic and earthquake nucleation effects," *Journal of Geophysical Research: Solid Earth*, vol. 120, pp. 5082–5103, July 2015.
- [50] J. H. Dieterich, "A constitutive law for rate of earthquake production and its application to earthquake clustering," *Journal of Geophysical Research*, vol. 99, no. B2, pp. 2601–2618, 1994.
- [51] M. Acosta, "Data and software for: Acosta et al., 2023," 2023. <https://doi.org/10.5281/zenodo.8329298>.
- [52] S. A. Shapiro, O. S. Krüger, and C. Dinske, "Probability of inducing given-magnitude earthquakes by perturbing finite volumes of rocks," *Journal of Geophysical Research: Solid Earth*, vol. 118, no. 7, pp. 3557–3575, 2013.
- [53] A. Boyet, S. D. Simone, S. Ge, and V. Vilarraza, "Poroelastic stress relaxation, slip stress transfer and friction weakening controlled post-injection seismicity at the Basel Enhanced Geothermal System," *Commun Earth Environ*, vol. 4, no. 104, 2023.
- [54] H. Meyer, J. D. Smith, S. Bourne, and J.-P. Avouac, "An integrated framework for surface deformation modelling and induced seismicity forecasting due to reservoir operations," *Geological Society, London, Special Publications*, vol. 528, no. 1, pp. 299–318, 2023.

- [55] T. Gustafsson and G. D. McBain, "scikit-fem: A Python package for finite element assembly," *Journal of Open Source Software*, vol. 5, no. 52, p. 2369, 2020.
- [56] L. F. Shampine and M. W. Reichelt, "The matlab ode suite," *SIAM Journal on Scientific Computing*, vol. 18, no. 1, pp. 1–22, 1997.

APPENDIX I MODEL IMPLEMENTATION

For ease of implementation and visualization, and without losing the effectiveness of the theoretical results shown in Section III, the 3D diffusion equation (4) was implemented in a 2D version using a depth average approach (see [34], [54] for other examples of depth averaging). The depth averaging was performed as follows

$$\begin{aligned} \frac{1}{h(x)} \int_0^{h(x)} u_t(x, t) dx_3 &= -\frac{1}{\beta h(x)} \int_0^{h(x)} \nabla q(x, t) dx_3 \\ &+ \frac{1}{\beta h(x)} \int_0^{h(x)} \sum_{i=1}^n \mathcal{B}_i(x) Q_i(t) dx_3 \\ &= -\frac{1}{\beta h(x)} \int_0^{h(x)} \nabla q(x, t) \cdot \hat{e}_1 dx_3 \\ &- \frac{1}{\beta h(x)} \int_0^{h(x)} \nabla q(x, t) \cdot \hat{e}_2 dx_3 \\ &- \frac{1}{\beta h(x)} \int_0^{h(x)} \nabla q(x, t) \cdot \hat{e}_3 dx_3 \\ &+ \frac{1}{\beta h(x)} \sum_{i=1}^n \hat{\mathcal{B}}_i(\hat{x}) Q_i(t), \end{aligned}$$

where $h(x)$ is the depth of the reservoir, \hat{e}_i are the unit vectors in the x_i direction, $\hat{\mathcal{B}}_i(\hat{x}) = \int_0^{h(x)} \mathcal{B}_i(x) dx_3$ and the new space variable $\hat{x} \in \mathbb{R}^2$, $\hat{x} = [x_1, x_2]^T$ is defined. We note that $\int_0^{h(x)} \nabla q(x, t) \cdot \hat{e}_3 dx_3 = 0$ due to the BC of the reservoir, $q(x, t) \cdot \hat{e} = 0 \quad \forall x \in S$. Defining the depth average pressure as $\hat{u}(\hat{x}, t) = \frac{1}{h(x)} \int_0^{h(x)} u(x, t) dx_3$, and the average flux as $\hat{q}(\hat{x}, t) = \frac{1}{h(x)} \int_0^{h(x)} \nabla q(x, t) \cdot (\hat{e}_1 + \hat{e}_2) dx_3$, the last expression becomes

$$\hat{u}_t(\hat{x}, t) = -\frac{1}{\beta} \nabla \hat{q}(\hat{x}, t) + \frac{1}{\beta h(x)} \sum_{i=1}^n \hat{\mathcal{B}}_i(\hat{x}) Q_i(t). \quad (46)$$

For the case of the SR equation in (6), the average SR, $\hat{R}(\hat{x}, t)$, was obtained from the system

$$\hat{R}_t(\hat{x}, t) = \hat{R}(\hat{x}, t) \left\{ -\gamma_1(\hat{x}, t) \hat{u}_t(\hat{x}, t) - \gamma_2(\hat{x}, t) [\hat{R}(\hat{x}, t) - R^*] \right\}. \quad (47)$$

Note how systems (4) and (46), and (6) and (47) have finally the same form, allowing the theoretical developments of section III to be applied without changes. The 2D diffusion equation (46) is numerically solved in Section IV using finite elements [55]. Triangular mesh was used to obtain 446 elements (see Fig. 15). Then, both systems (46)–(47) were discretized in time using an implicit algorithm [56].

ACKNOWLEDGMENTS

The authors would like to acknowledge the European Research Council's (ERC) support under the European Union's Horizon 2020 research and innovation program (Grant agreement no. 101087771 INJECT). The first author would also like to thank the Region Pays de la Loire and Nantes Métropole for their support under the Connect Talent programme (CEEV:

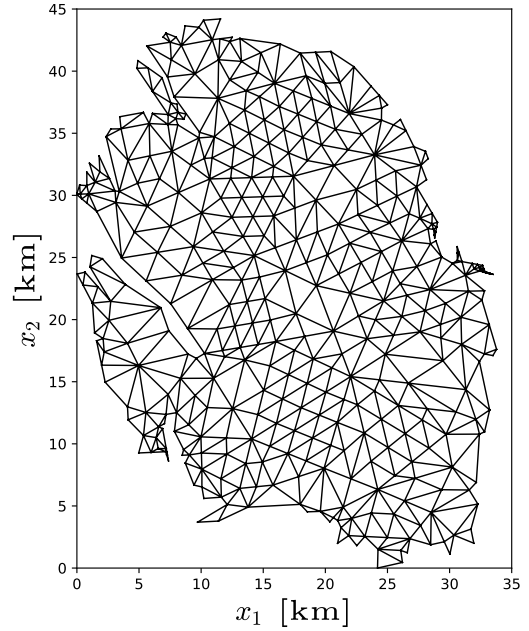


Fig. 15. Discretization of the reservoir in 446 elements using triangular mesh.

Controlling Extreme EVents - Blast: Blas LoAds on SStructures). Both authors would like to express their grateful thanks to Dr. Mateo Acosta for their fruitful discussions about the Groningen reservoir and related data.



Diego Gutiérrez-Oribio was born in Mexico and received his M.S. degree and Bachelor degree in Mechatronic Engineering from the National Autonomous University of Mexico (UNAM), Mexico City, Mexico in 2016 and 2013, respectively. In 2021, he received his Ph.D. in Electrical Engineering - Automatic Control (with honours) at UNAM. He is currently a post-doctoral member in the GeM Laboratory in the Ecole Centrale, Nantes, France. His current research of interests include the control of mechanical systems, non-linear control, sliding-mode control, reinforcement learning and control of earthquake phenomena.



Ioannis Stefanou is Professor at ENSTA Paris, Institut Polytechnique de Paris, France. He studied civil engineering, mechanics and applied mathematics at the National Technical University of Athens. He then did his PhD thesis at the Laboratory of Geomaterials of the same institution. His main research topics are mechanics, machine learning and control theory with applications to geomechanics, structural dynamics and earthquake control. He was the PI of the ERC-StG project "Controlling earthQuakes - Co-Quake" (www.coquake.eu), of the Connect Talent project "Controlling Extreme EVents - CEEV" (www.blastructures.eu) awarded by the Pays de la Loire. Currently, he is the PI of the ERC-CdG project "Preventing human-induced seismicity to fight climate change – INJECT".